Top Curr Chem (2013) 335: 23–70
DOI: 10.1007/128_2011_229
© Springer-Verlag Berlin Heidelberg 2011
Published online: 25 October 2011

Dynamic Nuclear Hyperpolarization in Liquids

Ulrich L. Günther

Abstract Nuclear magnetic resonance (NMR) spectroscopy is a broadly used analytical method with major applications in chemistry, biochemistry and medicine. Key applications include structural analysis of small molecules, metabolites, larger biomolecules such as proteins, RNA and DNA, and applications in material science. Magnetic resonance imaging (MRI), which is based on the same physical principles, is extensively used in medical diagnostics and represents the most widespread application of NMR. However, NMR is fundamentally limited in sensitivity and this has always restricted its applicability. Hyperpolarization techniques such as dynamic nuclear polarization (DNP) have become a major field of research and development because they hold the promise of increasing the sensitivity of NMR by several orders of magnitude. Such sensitivity enhancements could significantly broaden NMR applications, combining its unique structural information with much higher sensitivity. Unfortunately, there is no single implementation of DNP that would be suitable for a broader range of typical NMR applications. Experimental conditions often circumscribe areas of possible applications. Nevertheless, recent developments point towards experimental protocols providing solutions for specific applications of NMR. This review summarizes the concepts behind DNP in the light of recent developments and potential applications.

Keywords DNP • Dynamic Nuclear Polarization • Hyperpolarization • NMR

Dedicated to Heinz Rüterjans on the occasion of his 75th birthday.

U.L. Günther (✉)
HWB-NMR, School of Cancer Sciences, University of Birmingham, Vincent Drive, Edgbaston, Birmingham B15 2TT, UK
e-mail: u.l.gunther@bham.ac.uk

Contents

Abbreviations

CE	Cross effect
CIDNP	Chemically induced dynamic nuclear polarization
D-DNP	Dissolution DNP
DNP	Dynamic nuclear polarization
MRI	Magnetic resonance imaging
NMR	Nuclear magnetic resonance
O-DNP	Overhauser-DNP
OE	Overhauser effect
PHIP	Parahydrogen-induced polarization
QRP	Quantum rotor polarization
SE	Solid effect
SS-DNP	Solid-state DNP
TM	Thermal mixing

1 Introduction

1.1 Polarization

The widespread success of NMR spectroscopy arises from its vast information content and the predictability of spectra based on the solid theoretical framework underlying NMR [1]. However, NMR remains limited in sensitivity, as a direct consequence of the small energy difference between nuclear spin states. For $i = 1/2$ spins such as protons, ^{13}C, ^{15}N, ^{31}P, ^{19}F and other nuclei, the energy difference that determines the population of the two spin states α and β is $\Delta E = \gamma \hbar B_0$, where

γ is the gyromagnetic ratio and B_0 the magnetic field. This energy difference determines the population of spin states. Polarization is commonly defined as [2]:

$$P = \frac{n_\beta - n_\alpha}{n_\beta + n_\alpha} = \tanh \frac{\gamma \hbar B_0}{2kT}. \quad (1)$$

Equation (1) highlights the limitations of NMR: At the magnetic field of the largest NMR magnets available today, with $B_0 \approx 23.5$ T, equivalent to 1,000 MHz of proton frequency, the polarization is still only ≈80 ppm (0.008%). According to (1), polarizations are much higher at lower temperatures. At a temperature of 1 K the polarization of protons reaches 2.4% for 23 T, indicating a possible avenue for reaching higher polarizations. However, owing to its much larger gyromagnetic moment, unpaired electrons reach high polarizations at modest field strengths and temperatures below 10 K. DNP builds on the transfer of this high spin polarization from electrons to nuclear spins.

1.2 Hyperpolarization Methods

Besides DNP, there are several alternative routes towards increasing polarizations, building on a range of different experimental concepts. An obvious way towards larger polarizations lies in brute force methods. In principle, increasing the magnetic field falls into this category. This has been the method of choice in the past two to three decades, with the largest superconducting high-resolution NMR magnets now at 23.5 T. However, magnetic fields required to reach polarizations of 10–20% are far outside the window of what is currently feasible with superconducting magnets.

Brute force by lowering temperatures is a reasonable alternative for polarizing nuclear spins. At 0.1 K the polarization of protons reaches 23%. In practice, this is of course limited by the difficulty of reaching such low temperatures. Moreover, spectra of frozen samples need to be recorded with low-temperature magic angle spinning (MAS), which is technically enormously challenging at such temperatures. Alternatively, samples may be heated to ambient temperatures after polarization to acquire a high-resolution spectrum in the liquid state, a procedure that may well be feasible. There are, however, serious limitations to low temperature Boltzmann polarization, as the processes driving the polarization build-up will become very slow.

In another class of experiments, hyperpolarized states are generated by spin-sensitive chemical reactions. These include para-hydrogen-induced polarization (PHIP) [3–5] and chemically induced dynamic nuclear polarization (CIDNP) [6–8]. The latter involves non-equilibrium nuclear spin state populations that are produced in chemical reactions that proceed through radical pair intermediates. CIDNP's applicability has been focused towards the study of chemical reactions and the detection of surface exposed residues in proteins [9], but has so far remained limited to specialized chemical systems.

PHIP arises from quantum mechanical spin rotational states in diatomic hydrogen. Employing chemical reactions, these states can be used to generate molecules with enormously high spin polarizations. This is usually achieved by a hydrogenation reaction using para-hydrogen on an unsaturated organic molecule. The advantage of PHIP is that a theoretical 100% of ^{1}H polarization is feasible. PHIP has experienced a significant revival following recent developments by Duckett using a reversible approach whereby polarization is transferred via a metal centre [10], thus eliminating the need for an unsaturated analogue of the substrate. This approach now considerably broadens the applicability of PHIP as a general polarization method in solution and represents a competitive approach to DNP-NMR.

Quantum rotor polarization (QRP) has been known for a long time following pioneering work by Haupt in the 1970s [11]. QRP arises from rotational hindrance in methyl groups, giving rise to quantum tunneling. Large and rapid temperature jumps change the population of rotational energy levels and this process is associated with spin changes through the influence of the exclusion principle (reviewed in [12]). QRP can be seen as an equivalent to PHIP for molecules with C3 symmetry. Recently, new applications based on QRP have been explored by several groups [13–16], showing applicability beyond the narrow range of molecules known to exhibit such effects, if temperatures below 4 K are used [13]. QRP is also relevant for some variants of DNP as there the two mechanisms develop simultaneously and can interfere constructively or destructively.

Polarization of spins can also be achieved by optical pumping with circularly polarized laser light, primarily polarizing alkali metals (typically Rb), followed by spin exchange to noble gases (e.g., Rb–Xe spin exchange) [3, 17, 18]. Although limited to some noble gases, optically hyperpolarized ^{129}Xe and ^{3}He (both spin 1/2 nuclei) in the gas phase can be used for magnetic resonance imaging (MRI), either by using Xe directly [19] or by employing a nuclear Overhauser effect (NOE) to alter the polarization of nuclear spins [20]. Moreover, hyperpolarization of ^{83}Kr with spin 9/2 via Rb has been demeonstrated by Meersman and coworkers using natural abundance Kr containing 11.5% of the ^{83}Kr isotope [178].

Another method of polarizing nuclear spins is dynamic nuclear polarization (DNP), whereby the comparably large electron spin polarization (see Fig. 1) is transferred to nuclear spins by saturating the electron resonance. DNP is almost as old as NMR spectroscopy, building on the aforementioned theoretical work by Overhauser [21] who predicted what is today known as the Overhauser effect (OE). DNP was soon after demonstrated experimentally by Carver and Slichter [22, 23]. The enhancement, ε, that can be obtained by DNP is determined by the gamma ratio γ_e/γ_n, which is 660 for protons and 2,625 for ^{13}C.

DNP in the solid state, via the solid effect (SE) can be traced back to Pound [24], Abragam [25] and Jeffries [26]. Borghini described DNP in a spin temperature model [27, 28], which led to the discovery of thermal mixing (TM) [29]. In 1963 [30, 31], the cross effect (CE) was described, and later verified by Hwang, Hill [32, 33] and Wollan [34, 35]. In the following years, major work was carried out by Wind and coworkers [36]. Hausser and Stehlik derived the framework for DNP in

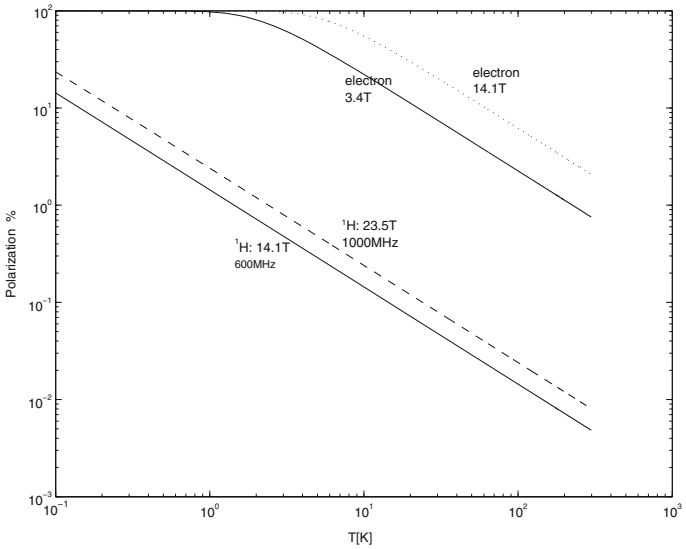

Fig. 1 Polarization levels as a function of temperature for ^{1}H at 14.1 T (600 MHz) and 23.5 T (1 GHz), and for electrons at 3.4 T and at 14.1 T, calculated using (1)

liquids [37], while Griffin [38] developed a major body of work leading to applications of DNP in solid state NMR using MAS.

The development of nuclear hyperpolarization has seen a significant revival in recent years, with major new developments in various hyperpolarization methods. This review focuses on DNP in liquids with the primary goal of providing an overview of the current state-of-the-art and the feasibility of applications arising from new developments. There are a number of reviews on DNP in liquids by Hausser and by Müller-Warmuth [37, 39], and a recent review by Bennati primarily focused on Overhauser DNP [40]. Early reviews include a chapter in a monograph by Abragam [1], and a review on the solid effect by Jeffries [2]. Abragam and Goldman published a fundamental review of theoretical concepts in 1972 [41]. More than 10 years later, Wind reviewed the developments of solid-sate DNP [36], summarizing the underlying theoretical concepts. A more recent review by Griffin provides a comprehensive overview of DNP principles and instrumentation [42].

The focus of this review is on DNP methods with applications in liquids. This includes dissolution DNP, which is of course strictly a solid-state polarization method although targeted towards NMR spectroscopy or imaging in the liquid state.

2 Overview Over DNP Mechanisms

Dynamic nuclear polarization describes a process whereby spin polarization is transferred from unpaired electrons to nuclear spins. This process exploits the much larger polarizations arising from electrons, which can be close to 100% at

sufficiently low temperatures [see (1) and Fig. 1]. The choice of the transfer mechanism depends on the experimental conditions, whether the polarization is carried out in liquids or solids, and the choice and concentration of radicals. The transfer of polarization is initiated by irradiation at or close to the electron Larmor frequency, and the transfer involves simultaneous nuclear and electron spin transitions, during the irradiation or induced by relaxation.

The overall Hamiltonian of an electron-nuclear spin system in a magnetic field is given by:

$$H = \omega_e S_Z - \omega_n I_Z + H_{ee} + H_{en} + H_{nn}. \tag{2}$$

The first two terms describe the electron and nuclear Zeeman interactions, respectively, with $\omega_e = \gamma_e B_0$ and $\omega_n = \gamma_e B_0$, where γ_e and γ_n are the gyromagnetic ratios of electrons and nuclei, respectively, and B_0 represents the external magnetic field strength. S and I are used for electron and nuclear spin operators, respectively. For indices, this review always uses n for nucleus and e for electrons, i.e., $\gamma_S = \gamma_e$ and $\gamma_I = \gamma_n$.

H_{ee}, H_{en} and H_{nn} denote the spin–spin interactions between electrons, between electrons and nuclei, and between nuclei, respectively. H_{ee} has often been neglected for sufficiently dilute concentrations of electrons. It becomes, however, relevant for the solid state DNP mechanisms (SE, TM and CE); in the case of the CE a specific electron–electron interaction can be utilized to optimize the DNP enhancement. It is also possible that electron relaxation is important for polarizations carried out at very low temperatures.

Abragam and Goldman recognized that the dipolar interaction causing relaxation between nuclei determines the polarization time in the solid state. Nuclear relaxation is also relevant in solution, as will be shown in 2.1. Moreover, recent work by Vega has paid attention to nuclear spin diffusion associated with DNP, the key mechanism for transfering magnetization from molecules in contact with the radical to other nuclei in the solid state [43].

In solution, the term that seems most important for DNP is H_{en}, describing the electron–nuclear interactions, which are governed by the dipolar interaction H^D and the scalar Fermi contact interaction H^{Sc}, where:

$$H_{en}^D = \frac{\gamma_n \gamma_e \hbar}{r_{jk}^3}[I \cdot S - 3(I \cdot n)(S \cdot n)], \tag{3}$$

where r is the distance between the electron and the nucleus and $\boldsymbol{n} = \boldsymbol{r}/\mathrm{r}$ is the unit vector in the direction joining centres of the two particles.

In high magnetic field, the non-secular part is often discarded leaving solely the secular part of (3):

$$H_{en}^D = \frac{\gamma_n \gamma_e \hbar}{r_{ij}^3}[I \cdot S - 3I_z S_z]. \tag{4}$$

The Hamiltonian for the scalar Fermi contact can be written as:

$$H_{\text{en}}^{\text{Sc}} = I \cdot A \cdot S, \tag{5}$$

where A represents the scalar hyperfine coupling tensor.

All mechanisms of DNP share the common principle of transferring polarization from electrons to nuclei, following irradiation at or near the frequency of the ESR line of the electron. The DNP process depends essentially on the magnitude of the hyperfine and dipolar interactions. However, this process only determines the polarization of nuclei in close proximity to an electron, the core nuclei. In liquids, this polarization transfer is driven by relaxation, following excitation of electron transitions. In solids, transitions are directly driven by microwave irradiation.

For the DNP process to proceed from an initial polarization zone, it is essential that polarization be either transported to other nuclei via spin diffusion, as is the case in the solid state. Alternatively, in liquids unpolarized nuclei become available by translational diffusion. These two options are responsible for largely different polarization processes in (insulating) solids as compared to liquids (and metals). In liquids, this process is fundamentally different, and rotational and translational diffusion processes govern the polarization process, as originally described by Hausser et al. [37], Müller-Warmuth et al. [39] and others. Relaxation processes are driven by the time dependence of the overall Hamiltonian, arising form variations in the vector $\boldsymbol{r}$ and the hyperfine coupling constants, causing relaxation transitions between the spin states.

The choice of the polarization mechanism depends entirely on the experimental conditions. Overhauser DNP is the only DNP mechanism known to work in liquids. The specific mechanism in the solid state depends primarily on the experimental conditions, i.e., choice and concentration of the radical. Table 1 summarizes the DNP mechanisms and the conditions required for these mechanisms. The key mechanisms will be reviewed in the following paragraphs.

DNP can also be classified by the experimental arrangement that is used to carry out the experiment. In this sense three technical implementations of DNP prevail:

1. Overhauser DNP (O-DNP), driven by the Overhauser effect (OE), where the entire process is carried out in the liquid state.
2. Solid-state DNP (SS-DNP) at low temperatures (typically 90 K), driven by the cross effect (CE), using high-power microwave sources in conjunction with MAS for solid-state NMR.
3. Dissolution DNP or ex situ DNP (D-DNP), typically carried out at temperatures $<$1.5 K, driven by thermal mixing (TM) or the solid effect (SE). The polarized liquid sample is generated by sample dissolution and is transfer to an analytical NMR magnet to acquire a spectrum.

Significant progress in DNP arises from improved instrumentation, mainly from high power microwave sources that have become available in recent years. These developments were much influenced by Griffin's pioneering work using gyrotron

Table 1 Common DNP mechanisms

Underlying mechanism	OE	SE	CE	TM
Common application	O-DNP (liquids)	D-DNP	SS-DNP	D-DNP
Sample type	Liquids; alkali metals; organic conductors	Glassy samples in the solid state	Glassy samples in the solid state	Glassy samples in the solid state
Conditions	H_{en} time-dependent $\approx\omega_e^{-1}$; polarization transfer via relaxation, depending on scalar and dipolar interaction.	H_{en}^{Sc} causes mixing of states $\Rightarrow$ forbidden transition, slow build-up Low concentration of radicals, no dipolar coupling between radicals	Inhomogenous broadening of the ESR signal, large g-anisotropy, dipolar coupling between radicals. Optimal with biradicals satisfying: $\omega_n = \omega_{eS1} - \omega_{eS2}$	Homogenous broadening[a] of the ESR signal, small g-anisotropy High concentration of radicals
		$\Delta\omega_{e1/2} \ll \omega_n$ Unresolved SE for $\omega_{e1/2} \approx \omega_n$	$\Delta > \omega_n > \omega_{e1/2}$ $\Rightarrow$ resolved hyperfine lines in ESR spectrum	$\omega_{e1/2} > \omega_n$
Frequency dependence	$\omega_e\tau_c < 1$	$\sim B_0^{-2}$	B_0^{-1}	$\omega_{e1/2}$
Microwave irradiation frequency for maximal enhancement	$\omega = \omega_e$	$\omega = \omega_e \pm \omega_n$ Maxima in microwave sweep separated by $2\omega_n$	ω_{max} at polarization maximum, depends on EPR line shape	ω_{max} at polarization maximum, depends on EPR line shape $\omega \approx \omega_e \pm \omega_{e1/2}$

ω_e electron Larmor frequency, ω_n nuclear Larmor frequency, $\omega_{e1/2}$ homogenous half width of the ESR signal, Δ inhomogenous breadth of the EPR spectrum, τ_c electron rotational correlation time.
[a]The expressions homogenous and inhomogenous broadening are commonly used in EPR spectroscopy, but are less familiar to NMR spectroscopists. Inhomogeneous broadening of the ESR spectrum describes a signal composed of a large number of narrower spectra, arising from different hyperfine couplings, each shifted with respect to each other. In the case of homogeneous broadening, the linewidth of the ESR spectrum is determined by the electron relaxation times

sources for SS-DNP [42]. Another important technological development is that of D-DNP by Ardenkjær-Larsen [44], which yields by far the largest overall enhancements and has major applications in MRI. Moreover, recent work on O-DNP shows an avenue towards applications of DNP in solutions. Implementations of O-DNP come in different flavors, either carrying out the polarization at the same field strength as the NMR measurement or polarizing at lower field and transporting the sample to higher field for the NMR measurement.

2.1 Overhauser DNP

The OE was first described theoretically in a 1953 landmark paper by Albert Overhauser, who predicted for metals that "if the electron spin resonance of the conducting electrons is saturated, the nuclei will be polarized to the same degree they would if their gyromagnetic ration were that of the electron spin"[21]. In the same year, this theoretical concept was verified by Carver and Slichter for metallic lithium dispersed in oil, resulting in an enhancement factor of 100-fold [22]. Figure 2 shows the first DNP spectrum from a 1953 publication by Carver and Slichter [22]. Later the same authors demonstrated the DNP effect for ^{23}Na and ^{1}H in sodium ammonia solutions [23]. The history of these early DNP experiments was recently reviewed by Slichter [45].

Although O-DNP was originally discovered in alkali metals, its main application today is in DNP in solution, predominantly for ^{1}H and for ^{13}C NMR, although many other spin 1/2 nuclei can be polarized. Earlier applications also included ^{1}H and ^{13}C DNP of organic conductors [46–48].

The O-DNP experiment requires irradiation at the electron Larmor frequency to saturate the electron transition. The enhancement arises from subsequent relaxation processes involving simultaneous reversals of I and S in opposite directions (flip-flop transitions, W_0), or in the same direction (flip-flip transitions, W_2). This is depicted by the energy level diagram in Fig. 3. Hausser and Stehlik introduced a phenomenological description using rate equations [37], based on Solomon's treatment of the OE. According to the Solomon equations [49], the rate equation for the expectation value of the nuclear polarization $<I_z>$ can be written as:

$$\frac{\mathrm{d}\langle I_z\rangle}{\mathrm{d}t} = -\rho(\langle I_z\rangle - I_0) - \sigma(\langle S_z\rangle - S_0), \tag{6}$$

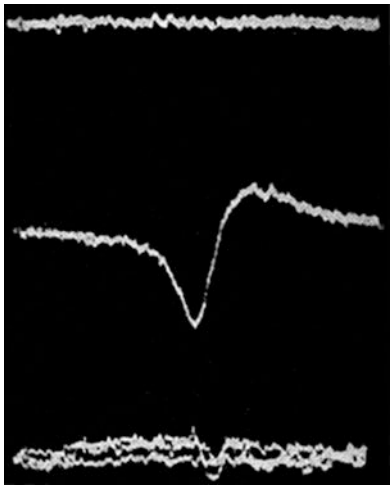

Fig. 2 Original DNP experiment performed by Carver and Slichter [22]. *Top*: The noisy ^{7}Li resonance. *Middle*: The ^{7}Li resonance enhanced by electron saturation. *Bottom*: Proton resonance in glycerin sample. (Copyright 1953 by The American Physical Society)

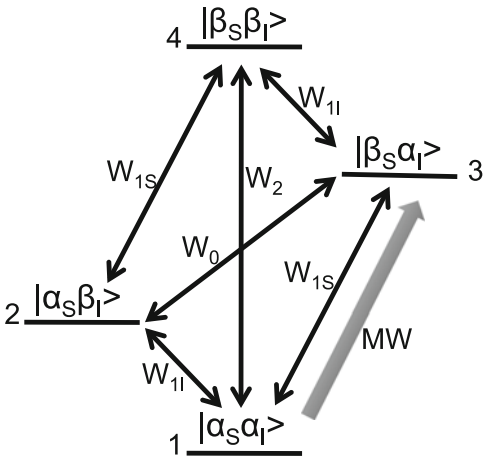

Fig. 3 Energy level diagram for a two-spin system; *S* represents the electron and *I* a spin 1/2 nucleus. Transitions are labelled with the respective transition probabilities: W_{1S} and W_{1I} are the transition probabilities for the electron *S* and for the nucleus *I*, respectively. W_0 and W_2 represent the zero and double quantum transition probabilities, respectively

where I_0 and S_0 represent the values of $<I_z>$ and $<S_z>$ in thermal equilibrium. Hausser introduced three key parameters, the coupling factor ξ, the leakage factor f and the saturation factor s [37]:

$$\xi = \frac{\sigma}{\rho} = \frac{W_2 - W_0}{W_0 + 2W_1 + W_2}, \tag{7a}$$

where σ is the cross-relaxation and ρ the auto-relaxation rate,

$$f = \frac{\rho}{\rho + W_{1I}^0}, \tag{7b}$$

$$s = \frac{S_0 - \langle S_z \rangle}{S_0}. \tag{7c}$$

The coupling factor describes the contribution of the transition probabilities W_i towards the maximum polarization and depends on the nature of the short range interactions that determine these transition probabilities.

The overall DNP enhancement has been defined as:

$$\epsilon = \frac{\langle I_z \rangle}{I_0} = 1 - \xi \cdot f \cdot s \frac{|\gamma_e|}{\gamma_n}. \tag{8}$$

It should be noted that the commonly used NOE factor is defined differently as $\frac{I_z - I_0}{I_z} = 1 - \epsilon = \xi \cdot f \cdot s \frac{|\gamma_e|}{\gamma_n}$. Some authors defined their DNP enhancement this way. If f and s both have a value of +1 the enhancement is $\epsilon = 1 - \xi \frac{|\gamma_e|}{\gamma_n}$, i.e., a sufficiently large positive enhancement reflects a negative coupling factor.

The leakage factor f measures the contribution of the electrons towards the relaxation of the nuclei. (W_{1I}^0 in (7b) is the longitudinal relaxation rate of the

nucleus in the absence of a radical). It can be determined by relaxation measurements in the presence and absence of the radical. Values can range from 0 (no contribution from the radical) to 1 (relaxation controlled by the radicals). For nitroxide radicals it usually assumes a value close to 1 at radical concentrations of 10–20 mM.

The saturation factor s is a measure of the degree to which the electron transitions are saturated. When the electron transitions are completely saturated, s takes a value of 1. It depends on the microwave power and the relaxation of the electrons. The saturation factor becomes significantly more complicated in radicals with several hyperfine lines (two for ^{15}N, three for ^{14}N), such as nitroxide radicals, where various relaxation mechanisms need to be considered if only one line is saturated. Bates and Drozdoski proposed a theoretical model taking into account electron spin exchange transitions [50], which has recently been extended by Armstrong [51] to account for the relaxation effect arising from ^{14}N (and ^{15}N) nuclei. Recently Türke and Bennati [179] proposed to measure saturation factors using pulsed electron–electron double resonance (ELDOR) experiments measuring the saturation level of a hyperfine line when pumping a coupled line of the nitroxide spectrum. For ^{15}N-^{2}H-labelled TEMPONE (4-oxo-2,2,6,6-tetramethylpiperidine-*N*-oxyl) radical, this study demonstrates a strong dependence of s on the concentration of the radical, owing to a predominant Heisenberg exchange mechanism at concentrations $\geq$5 mM. Almost complete saturation can be achieved in water by irradiating one electron paramagnetic resonance (EPR) transition. According to calculations by Armstrong et al., this may not be the case for ^{14}N-TEMPONE [51] (radicals are described in Sect. 3.4).

Hausser used a semi-classical approach to determine the dependence of σ and ρ on the spectral densities of molecular motions for different relaxation mechanisms (S for scalar, D for dipolar) [49]:

$$\rho_{\mathrm{S}} = -\sigma_{\mathrm{S}} = \left[\left(\frac{A^2}{2}\right) J_{\mathrm{S2}}(\omega_{\mathrm{n}} - \omega_{\mathrm{e}}) + \beta J_{\mathrm{S1}}(\omega_{\mathrm{n}})\right], \tag{9}$$

$$\rho_{\mathrm{D}} = \frac{\gamma_{\mathrm{n}}^2 \gamma_{\mathrm{e}}^2 h^2}{10 r_{\mathrm{en}}^6} [(6J_{\mathrm{D}}(\omega_{\mathrm{n}} + \omega_{\mathrm{e}}) + J_{\mathrm{D}}(\omega_{\mathrm{n}} - \omega_{\mathrm{e}}) + 3J_{\mathrm{D}}(\omega_{\mathrm{n}})], \tag{10}$$

$$\sigma_{\mathrm{D}} = \left(\frac{\gamma_{\mathrm{n}}^2 \gamma_{\mathrm{e}}^2 h^2}{10 r_{\mathrm{en}}^6}\right) [6J_{\mathrm{D}}(\omega_{\mathrm{n}} + \omega_{\mathrm{e}}) - J_{\mathrm{D}}(\omega_{\mathrm{n}} - \omega_{\mathrm{e}})], \tag{11}$$

with Lorentz-shaped scalar and dipolar spectral density functions for rotational diffusion [52]:

$$J_{\mathrm{S1,2}}(\omega) = \tau_{\mathrm{S1,2}}/(1 + \omega^2 \tau_{\mathrm{S1,2}}^2); \quad J_{\mathrm{D}}(\omega) = \tau_{\mathrm{D}}/(1 + \omega^2 \tau_{\mathrm{D}}^2). \tag{12}$$

The correlation times of the scalar and dipolar couplings are:

$$\tau_{\mathrm{S1,2}} = (1/\tau_{1,2} + 1/\tau_{\mathrm{e}})^{-1} \quad \text{and} \quad \tau_{\mathrm{D}} = (1/\tau_{\mathrm{e}} + 1/\tau_{\mathrm{r}})^{-1}. \tag{13}$$

In these equations, Hausser introduced the last term $\beta J_{S1}(\omega_n)$ in (9) to account for a time dependence of scalar relaxation by spin exchange, in which case electronic relaxation transitions induce pure nuclear relaxation transitions. β takes a value of 1 for $\tau_e \gg \tau_1, \tau_2$ and 0 for $\tau_e \ll \tau_1, \tau_2$. From these spin density functions and their contribution towards ρ and σ, the dependence of the coupling factor ξ can be calculated. Such curves are shown in Fig. 4.

These models are still limited by the restriction to rotational tumbling of both the electron and the nucleus. Müller-Warmuth and coworkers developed combined rotational and translational diffusion models (reviewed in [39]) for dipolar and scalar interactions, assuming independent diffusion of the molecules. They also developed a pulse diffusion model assuming occasional collisions between molecules, described via a Poisson process [39]. Later Hwang et al. [53] used force-free pair correlation functions to account for translational diffusion and ionic interactions for dipolar interactions, leading to the now commonly used equation:

$$J_{\text{trans}} = \frac{1 + \frac{5z}{8} + \frac{z^2}{8}}{1 + z + \frac{z^2}{2} + \frac{z^3}{6} + \frac{4z^4}{81} + \frac{z^5}{81} + \frac{z^6}{648}}, \quad \text{with } z = \sqrt{2\omega\tau_{\text{TD}}}, \tag{14}$$

where τ_{TD} is the correlation time for the translational diffusion constant, which has often been related to the closest distance between molecules d and to the diffusion coefficients D_I and D_S by $\tau_{TD} = d^2/(D_I + D_S)$. τ_{TD} and d can be determined by fast field-cycling relaxometry (NMR dispersion, NMRD) [54, 55]. Translational

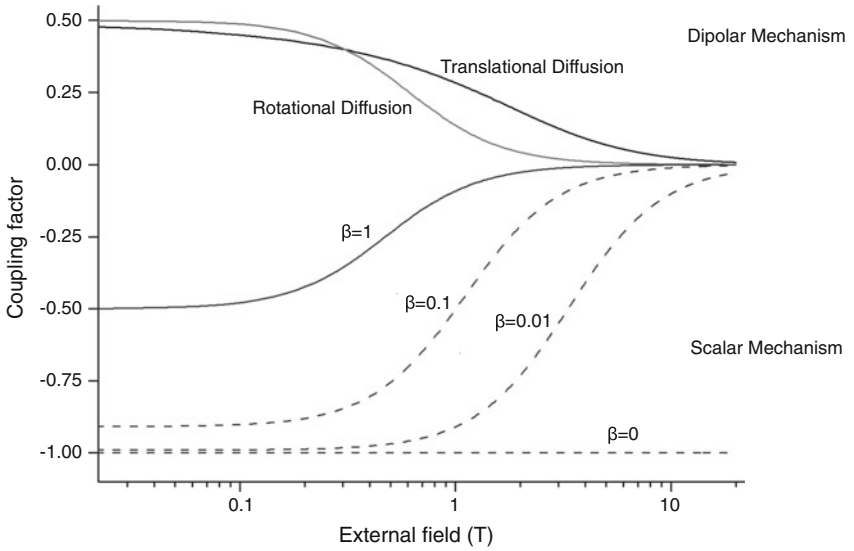

Fig. 4 Dependence of the coupling factor ξ derived from (9)–(13) on the magnetic field (and therefore on the Larmor frequency) for scalar and dipolar relaxation using spectral densities for rotational and translational diffusion using a correlation time of 20 ps (Reproduced from [40] with the permission of the Royal Society of Chemistry)

diffusion yields somewhat flatter curves than those for rotational diffusion, despite an overall similar behaviour (Fig. 4).

Overall, this treatment predicts that the scalar term for rotational diffusion is independent of double quantum relaxation (W_2) and depends only on zero quantum relaxation. The coupling factor ξ can assume values between 0.5 and -1.0 for pure dipolar and pure scalar relaxation, respectively. Moreover, the curves in Fig. 4 clearly show the expected field dependence with low values for the coupling factor, and therefore low enhancements for high magnetic fields.

The experimental behaviour of the saturation factor at low field (0.34 T) has been summarized by Müller-Warmuth [39] considering data up to 1983. The experimental curves for different nuclei and a series of radicals (Figs. 7, 8 and 10 in [39]) show a substantially more complex behaviour than the theoretical curves shown in Fig. 4 with mixed scalar and dipolar contributions. The scalar and dipolar contributions depend strongly on the nature of the sample, in fact on the specific nucleus, the solvent, and the choice of radical.

The relaxation mechanism encountered is therefore not predictable. As a general rule, protons have almost always shown a coupling factor driven by dipolar relaxation. Known exceptions are aromatic protons, for which Müller-Warmuth reported a weak scalar contact coupling, and acid protons of trifluroacetic acid [39]. For ^{13}C, positive and negative enhancements were reported. A more complex relaxation mechanism must be considered, particularly when the carbon is bound to a proton, in which case we have a three-spin system and possibly an additional ^{1}H/^{13}C-NOE. Most carbons seem to favour a dipolar mechanism (negative enhancement, positive ξ); recent examples include small molecules such as urea, acetone (CO and CH_3), pyruvate and methanol [56, 57], whereas *N*, *N*-dimethylformamide [57], chloroform [56] and other chlorinated sp3 carbons [39] showed a scalar coupling mechanism, as indicated by a positive enhancement and a negative ξ. Loening reported scalar relaxation for ^{31}P in triphenylphosphine, ^{13}C in carbontetrachloride, ^{15}N in aniline (opposite sign of the enhancement as $\gamma_N^{15} < 0$) and for ^{19}F in hexafluorobenzene. ^{31}P is an interesting case for studying the underlying effects, as trivalent phosphorus seems to favour a scalar relaxation mechanism, probably arising from lone pair interactions with the electron [39].

The temperature dependence of O-DNP has been the subject of recent discussions as it influences correlation times and the overall enhancement factor. The temperature dependence has been studied by NMRD measurements of water [54] and by molecular dynamics simulations [58], and more recently by measuring temperatures from the chemical shift change of the water resonance [59]. Temperature affects the saturation factor *s* by broadening the EPR lines of the TEMPONE nitroxide radical and, more importantly, the coupling factor ξ by the change of correlation times. These measurements showed a linear increase of the enhancement with temperature [59], in good qualitative agreement with the values of ξ from molecular dynamics simulations [58], but showed a significantly higher increase with temperature than previously expected. Bennati determined ξ using correlation times from NMRD measurements and found a somewhat more rapid variation with

temperature than those reported by Kryukov [59]. Overall, significant heating despite using small capillary samples (typically of nanolitre volumes) represents a major obstacle in a systematic analysis of the polarization parameters, which may have obscured previous results.

2.2 DNP via the Solid Effect

Soon after the discovery of DNP via the OE, Jeffries realized that "the saturation of so-called forbidden transitions will produce a comparable nuclear polarization directly in the sense that the applied radiofrequency field itself flips the nuclei" in solids [26]. He mentions that this had previously been observed by Pound [24] and theoretically considered by Abragam [25], who coined the name "l'effet solide." Jeffries later described the SE theoretically [60], and reviewed the early work of DNP in 1964 [2].

The SE is observed at low temperatures in solids for radicals with narrow EPR lines (typically trityl radicals), where the EPR linewidth is much smaller than the nuclear Larmor frequency ($\omega_{e1/2} \ll \omega_N$). As pointed out by Jeffries, it arises from driving the forbidden W_0 and W_2 as illustrated in Fig. 5.

DNP in the solid state follows a different mechanism compared to DNP in liquids, in particular at low temperatures, where the spatial parts of H_{en}^{D} and H_{en}^{Sc} become time-independent. Therefore, the enhancement is not driven by changes in polarizations arising from W_2 and W_0 relaxation, as is the case for O-DNP, but rather by driving these forbidden flip-flop (W_0) and flip-flip (W_2) transitions using microwave irradiation at the corresponding resonance frequencies $\omega_e + \omega_N$ or $\omega_e - \omega_N$, as shown in Fig. 6.

For this it is useful to expand the Hamiltonian (2) to include a term for the interaction of the electrons with the microwave field:

$$H = \omega_{0e} S_Z - \omega_{0n} \sum_i I_Z^i + 2\omega_{1e} S_Z \cos \omega t + \sum_i \mathbf{S} \cdot \mathbf{A}^i \cdot \mathbf{I}^i + H_{nn}. \qquad (15)$$

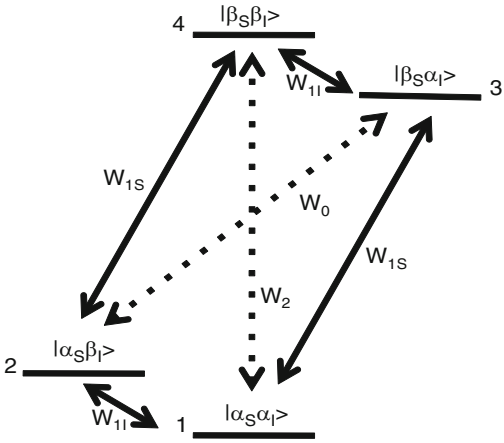

Fig. 5 Energy level diagram for the SE, which is driven by forbidden single and double quantum transitions (W_0 and W_2, *dotted lines*)

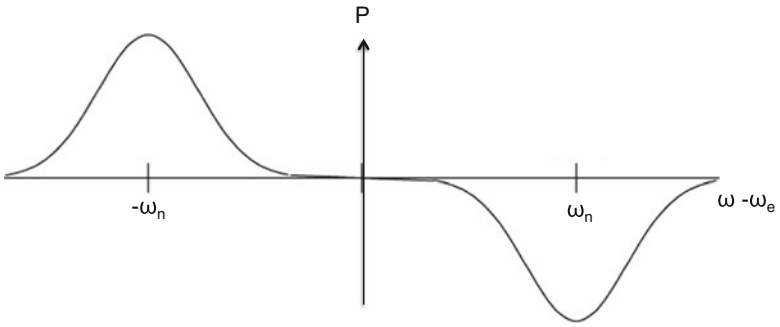

Fig. 6 Nuclear polarization by the SE as a function of the microwave frequency

The first and second term describe electron and nuclear Zeeman interactions, of the electron spin and the nuclear spins with the applied magnetic field, respectively, the third term the interaction of the electrons with the microwave field, and the fourth the hyperfine interaction between the nuclear spins. Here $\omega_{0e} = \gamma_e B_0$ is the electron Larmor frequency, with the applied magnetic field B_0 and the gyromagnetic ratio of the electron γ_e, and $\omega_{0n} = \gamma_n B_0$ the nuclear Larmor frequency with the nuclear gyromagnetic ratio γ_n. For the interaction of the electron spin with the microwave field B_1 we use $\omega_{1e} = \gamma_e B_1$. $\mathbf{A}^i$ represents the hyperfine tensor for the interaction between nuclei and electron spins. The term H_{nn} describing dipolar interactions between nuclear spins has been neglected in theoretical descriptions of the SE by Wenckebach [61, 62] and by Jeschke [63], but has been the subject of a recent theoretical treatment of coupled solid state DNP and spin diffusion using the density matrix formalism by Hovav and Vega [43].

The SE depends on non-secular terms of the electron-nuclear part of the Hamiltonian, leading to the mixing of states under the influence of microwave irradiation. This can easily be recognized by writing the Hamiltonian in a frame that points into the direction of the effective microwave field in which the z′ axis is defined by effective microwave frequency:

$$\omega_{\text{eff}} = \sqrt{(\omega_{0e} - \omega)^2 + \omega_{1e}^{s}} = \sqrt{\Delta^2 - \omega^2}. \tag{16}$$

Here, ω is the microwave frequency, and $\omega_{0e} - \omega$ represents the detuning of the microwave field with respect to the resonance frequency of the electron spin.

Polarization under the SE occurs when the Hartmann–Hahn condition $\omega_{\text{eff}} = \omega_n$ is fulfilled. The Hartmann–Hahn condition has two solutions $\Delta_{1,2} = \pm\sqrt{\omega_n^2 - \omega_{1e}^2}$, which yield maximum polarizations of opposite sign at the microwave frequencies $\omega_{\pm} = \omega_{0e} \pm \omega_n \cos(\Theta_{1,2})$, where the tilt angle of the effective field $\Theta_{1,2} = \mp\frac{\sqrt{\omega_n^2 - \omega_{1e}^2}}{\omega_n}$. For sufficiently large B_{1e} field strengths, Θ adopts small values and $\cos(\Theta) \to 1$, in which case $\omega_{1,2} \approx \omega_{0e} \pm \omega_n$.

The new Hamiltonian, ignoring the H_{nn} term for nuclear spin diffusion, and after several transformations into the tilted frame and averaged over a period of $2\pi\omega_{0n}^{-1} \approx 2\pi\omega_{eff}^{-1}$, thus satisfying the Hartmann–Hahn condition, we get:

$$H_{tilt,av} = Z + V_{zz}\cos\Theta + V_{\pm}\sin\Theta, \tag{17}$$

where

$$Z = \omega_{eff}S_{z'} + \omega_{0n}\sum_i I_z^i,$$

$$V_{ZZ} = \sum_i A_{zz}^i S_{z'} I_z^i$$

and

$$V_{\pm} = \tfrac{1}{4}\sum_i (A_{z+}^i S_+ I_-^i + A_{z-}^i S_- I_+^i).$$

The last term represents the flip-flop terms causing polarization transfer. Here, $S_{\pm} = S_{x'} \pm iS_{y'}$ and $I_{\pm} = I_{x'} \pm iI_{y'}$ are the step operators, and $A_{z\pm} = A_{zx} \pm iA_{zx}$ represents the tensor elements of the hyperfine coupling. The detailed transformation can be found in [61, 62]. Wenckebach developed this approach to describe coherent polarization transfer in the rotating frame; this is required for the nuclear orientation via electron spin locking (NOVEL) pulsed DNP experiment [64] in which a spin lock is applied to the electrons.

The transition probability for the forbidden transitions $W_{\pm}$ are given by:

$$W_{\pm} = 2\left|q_{ij}\right|^2 \pi\omega_e^2 f(\omega_e \pm \omega_n), \tag{18}$$

where q_{ij} are the coefficients that describe the degree of Eigenstate mixing $(q_{ij}|+>_i| + >_i)$, which is given by:

$$q_{ij} = -\frac{3}{4}\frac{\gamma_e\gamma_n\hbar}{\omega_n}\cdot\frac{1}{r_{ij}^3}\cdot\sin\theta_{ij}\cos\theta_{ij}e^{-i\phi_{ij}}. \tag{19}$$

$f(\omega_e \pm \omega_n)$ represents the normalized EPR lineshape function. In this equation, W_2 is proportional to q_{ij}^2 and therefore to ω_n^{-2} and B_0^{-2} (in contrast to CE and TM, which scale with B_0^{-1}) [36, 65]. This is thought to limit the use of the SE at higher field strengths.

If the ESR line is sufficiently narrow and the nuclear Larmor frequency sufficiently large $(\omega_n \gg \omega_{e1/2})$, polarization transfer occurs in two completely separated frequency regions, as shown in Fig. 6. In the case of the "differential solid effect" these lines are not as well resolved; consequently, the SE becomes inefficient, owing to simultaneous transitions of opposite sign that may cancel each other. This becomes relevant for low magnetic field strengths and for low γ nuclei. In practice, it may be hard to distinguish this situation from the thermal mixing DNP mechanism.

By solving rate equations similar to those used to describe the OE one can readily show under which conditions complete polarization becomes possible. Wind [36] derived the SE enhancement factor as:

$$\epsilon_{\mathrm{SE}} = 1 + \frac{W_2}{W_2 + W_{1I}} \cdot \left(\frac{\gamma_{\mathrm{e}}}{\gamma_{\mathrm{n}}} - 1 \right), \tag{20}$$

under the assumption that $W_{1\mathrm{e}}$ dominates the cross-relaxation rates W_2, W_0 and $W_{1\mathrm{n}}$ ($W_{1\mathrm{e}} \gg W_2, W_0, W_{\mathrm{n}}$). This enhancement becomes $\gamma_{\mathrm{e}}/\gamma_{\mathrm{n}}$ if cross-relaxation dominates the nuclear relaxation rate ($W_2 \gg W_{\mathrm{n}}$). The total enhancement is scaled by $\cos(\theta)$, where θ is the tilt angle of the effective field versus the static magnetic field, although θ will be small for sufficiently large magnetic field strengths.

Polarizations in the solid state work best in solid glass-forming solvents, such as glycerol, water, methanol, DMSO and certain mixtures of those. Deuteration considerably improves the polarization because it removes protons as the most important relaxation mechanism. It has also been shown that ^{13}C-enrichment of the glassy matrix with compounds like ^{13}C-acetone or ^{13}C-DMSO improves the polarization process, in some cases by enhancing the achievable polarization [66], for ^{13}C-DMSO and pyruvate by increasing the polarization rate [67]. These experiments highlight the importance of the spin diffusion barrier surrounding the paramagnetic centre [68], which has been the issue of recent theoretical considerations [43, 69]. Moreover, for polarizations at low temperature an additional relaxation mechanism arising from quantum rotor transitions in methyl groups must be considered [13, 70]. For polarizations of some substances this may dominate to a degree where the polarization arising from the CE may be completely quenched, although this effect can be eliminated by choosing the microwave frequency at $\omega_{\mathrm{e}} + \omega_{\mathrm{n}}$, where quantum rotor effects and DNP enhancements interfere constructively [70].

2.3 DNP via the Cross Effect and Thermal Mixing

The CE was discovered when Hwang examined Ley's radical (a bis-phenyl aroxyl radical) in polystyrene for increasing concentrations of the radical (0.25–5%) and found that the positive and negative DNP enhancement peaks move closer to each other for increasing concentrations of the same radical, as depicted in Fig. 7b [32, 33]. The underlying effect had previously been proposed by Abragam and Borghini [71] arising from spin–spin interactions between the electrons. A theoretical treatment by Wollan [35] also mentions an earlier discovery by Kessenikh [30, 31]. Despite its importance for SS-NMR, there is no comparable theoretical basis for CE as there is for the SE, although the basic requirements of the CE are reasonably well understood.

Both, the CE and TM require that the inhomogeneous EPR linewidth Δ is larger than the nuclear Larmor frequency ($\Delta > \omega_{\mathrm{n}}$), while the homogenous width must be

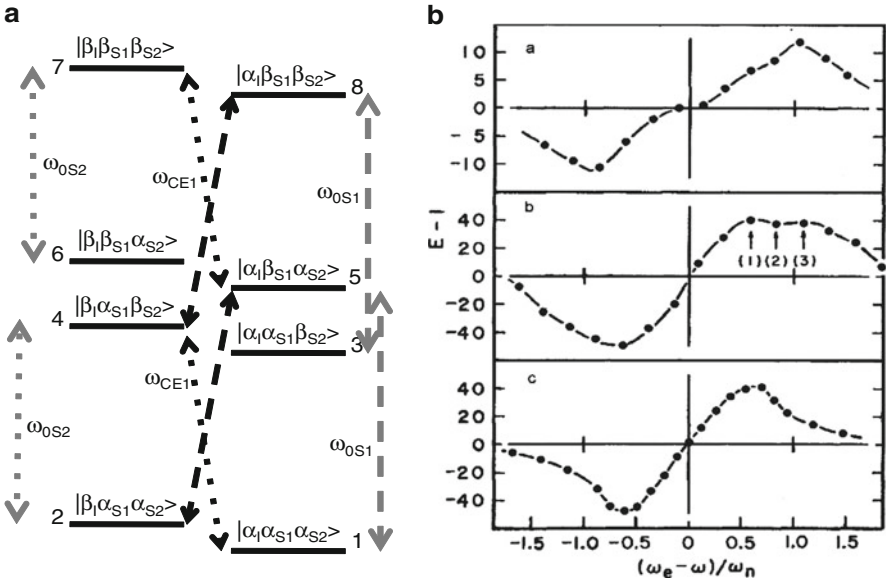

Fig. 7 (**a**) Energy level diagram for the CE, which requires a three-spin system with two electrons and one nucleus. Saturation of one of the EPR transitions for one of the dipolar coupled electrons (ω_{CE1} or ω_{CE2}) yields the enhancement for the nuclear transitions (ω_{0S1} for ω_{CE1} causing a negative enhancement, ω_{0S2} for ω_{CE2} causing a positive enhancement). (**b**) Polarization sweeps for protons obtained by Hwang et al. for increasing concentrations of Ley's radical in polystyrene. (0.25, 1.5 and 5%). The positive and negative DNP enhancement peaks move closer to each other for increasing concentrations of radical [32]. (Copyright 1967 by The American Physical Society)

smaller than the nuclear Larmor frequency ($\omega_{e1/2} < \omega_n$). For homogenously broadened EPR lines TM becomes active, for inhomogenously broadened lines CE is encountered. The latter is the case at higher fields and for larger g-tensors. The CE and TM are based on allowed transitions (Fig. 7a) and builds up polarization much faster than the SE.

Both effects require two or more electrons in close proximity. For CE, two electrons flip simultaneously with the nuclear spin via $|\beta_I\beta_{S1}\alpha_{S1}> \; |\alpha_I\alpha_{S1}\beta_{S1}>$ and $|\alpha_I\beta_{S1}\beta_{S2}> \; |\beta_I\alpha_{S1}\alpha_{S2}>$ transitions. This is achieved by irradiating at the frequency of one of the two radicals; as a consequence, both radicals and the proton flip. The matching condition for these transitions is $|\omega_{e1} - \omega_{e2}| \approx \omega_n$. This is the case when the levels 4 and 5 become degenerate, which can be approximated at high radical concentrations. Griffin and coworkers developed the concept of biradicals (such as TOTAPOL) for which the two electrons fulfill the matching condition. As the linewidth of EPR spectra scales with B_0, the effect scales with B_0^{-1} [42].

TM is similar to the CE but has been developed using a different theoretical model, specifically the concept of spin temperature based on the Provotov theory [1, 72], in which spin systems are treated as thermodynamic ensembles,

characterized by a spin temperature. This concept is suitable for describing a system with many electrons, where the Hamiltonian becomes too complex to determine individual Eigenlevels. This theory has recently been reviewed by Goertz [73], and has been applied to DNP spectra of solid deuterated butanol [74].

Qualitatively, TM can be interpreted as a transition from the CE towards an electron spin ensemble, arising from manifolds of states. TM requires high radical concentrations causing a homogenously broadened spectrum arising from strong electron interactions.

2.4 Pulsed DNP Methods

Pulsed DNP methods were recently reviewed [42]. Without doubt they offer significant advantages over classical DNP approaches. They do not scale as unfavourably with increasing field strengths, and have the potential to overcome some of the limitations encountered with SE, TM and CE. Pulsed methods include rotating frame DNP [65, 75], the integrated SE [76, 77], NOVEL [62, 64], the dressed SE [78] and a recently described method termed PONSEE (polarization of nuclear spins enhanced by ENDOR) [79]. NOVEL is a coherent method, which might have the potential to enable much faster polarizations, overcoming some of the limitations of the SE. However this requires irradiation at high power to fulfill a Hartmann–Hahn condition, which is not easily possible at higher field strengths with currently available microwave technology. Nevertheless, pulsed methods may have significant advantages for future experiments.

3 Experimental Implementations and Applications

The choice of experimental settings has largely been dictated by the constraints predicted by theoretical treatments, and by experimental limitations. SS-DNP is quickly becoming an important add-on to solid-state MAS-NMR spectrometers, building on Griffin's work using high power gyrotron microwave sources [80, 81]. These microwave sources open new avenues towards applications of DNP in biological systems. SS-DNP will not be covered in great detail because it is described in several excellent reviews by Griffin [42, 180]. The most important highlights of this work will, however, be summarized briefly in Sect. 3.1.

For DNP in solution, high power microwave irradiation is not necessarily the best possible concept owing to the heating effects in many solvents. Nevertheless, Prisner and coworkers have presented innovative designs for O-DNP at high field strengths, using a gyrotron as a microwave source (see Sect. 3.2.3) and showed that reasonably high enhancements are feasible. Several other authors have polarized samples at lower fields in solution and transported these samples to higher fields, either by flow injection or by shuttling samples or the probe (see Sects. 3.2.1 and 3.2.2).

These concepts will be presented in Sect. 3.2. A third revolutionary concept for DNP arises from work by Ardenkjær-Larsen, who designed an apparatus to polarize samples at temperatures below 1.3 K, which are, after rapid dissolution, transported into a higher field magnet (D-DNP). This version of DNP achieves by far the largest enhancements by combining a Boltzmann and a DNP enhancement, although the irreversibility of the dissolution process limits applications to one brief NMR experiment to be carried out during the T_1 relaxation time of the involved nuclei. Despite this limitation, D-DNP has become a highly popular implementation of DNP, driven by enormous enhancements of >10,000 and considerable successes in MRI applications. D-DNP will be covered in Sect. 3.3. This review will not cover the design of DNP probes and microwave sources, which have been reviewed elsewhere [42].

In this review, polarizers are classified according to common DNP implementations, as introduced above, specifically O-DNP for liquids, SS-DNP and D-DNP. This is, of course, artificial because the same microwave and radiofrequency sources can be used in liquids or in solution, except for the use of different cooling arrangements, MAS or a dissolution device. This classification is, however, useful to describe current experimental implementations.

3.1 SS-DNP

As SS-NMR is covered by several other reviews by Griffin and coworkers [42, 180], the current state will only be summarized briefly. Early implementations of DNP for SS-NMR were described by Wind [83] and later by Schaefer [84]. Wind built a SS-DNP MAS spectrometer using a 1.4 T magnet (60 MHz proton frequency), 15 MHz ^{13}C frequency and an ESR frequency of 40 GHz [83] using a 10 W Klystron working at a fixed microwave frequency. He reported spectra of BDPA-doped polystyrene, where he achieved enhancements of 26 for the direct polarization of ^{13}C and 130 for a cross-polarization from protons to ^{13}C. He found that the polarization develops via a SE for ^{1}H and TM for ^{13}C [36]. Wind also examined a range of coal samples and diamonds. An alternative design was presented by Schaefer and coworkers, who observed an enhancement factor of 20 for polystyrene doped with the BPDA radical [84]. Griffin conducted similar experiments in 1993 using a gyrotron operating at 140 GHz and a newly designed DNP-MAS probe [85, 86]. He also found that he could obtain higher polarizations by cross-polarization from ^{1}H to ^{13}C, and concluded that TM yields higher polarizations than direct polarization via the SE [86].

The introduction of gyrotron masers by Griffin was clearly a landmark for DNP. Using nitroxide radicals (4-amino-TEMPO, see Sect. 3.4) he showed in 1997 the first MAS SS-NMR spectra of a protein, ^{15}N-Ala-labelled T4 lysozyme, with an enhancement of ~50 [38]. Griffin realized not only that polarizations via the CE are more efficient than those via TM, he also found that CE benefits from the close proximity of electrons in biradicals, leading to about four-fold larger signal

intensities at much lower radical concentrations. He developed TOTAPOL, a water soluble biradical with a short linker [87, 88], which fulfills the need for a sufficiently strong dipolar coupling between the two electrons so that the difference between the electron Larmor frequencies approximates the nuclear Larmor frequency ($\omega_n = \omega_{e1} - \omega_{e2}$). With this concept, enhancements at 5 T and 90 K were increased from $\epsilon \sim 175$ to $\epsilon \sim 290$.

The search for optimal biradicals continues: more rigid radicals were shown to yield even larger enhancements [89], and recently a range of dinitroxides has been characterized [90]. Others have shown advantages for triradicals (DOTOPA-TEMPO) [91]. Thurber also demonstrated the advantage of lower temperatures for SS-DNP. The quest for even higher field strengths continues with gyrotron-based SS-DNP NMR spectrometers of up to 263 GHz (400 MHz proton frequency).

SS-DNP has become an important add-on to SS-NMR, with applications in protein NMR, as demonstrated for membrane proteins [92], amyloid fibrils [93] and an SH3 signalling protein [94]. However, the latter study by Oschkinat and Griffin also highlights the problems still encountered with SS-DNP for proteins. Deuteration was required to achieve any decent enhancement and the enhancement factor drops from ~70 to ~10 between 98 and 178 K. However, DNP at 98 K is impractical as the resolution at this temperature is insufficient for assignments.

Griffin has generally polarized protons with subsequent polarization transfer to ^{13}C. For many molecules this proved to be the right choice, despite the lower theoretical γ_e/γ_n ratio for protons (660) versus ^{13}C (2,625). However, Griffin's recent work shows that larger enhancements are possible by polarizing ^{13}C directly, although at the expense of a longer polarization time (~5 s for ^{1}H, 114–176 s for glycerol) [95], as a consequence of slower propagation of polarization for ^{13}C owing to the smaller dipolar coupling for ^{13}C compared to ^{1}H. Another option demonstrated by the same group is cross-polarization from ^{2}H to ^{13}C, which benefits from a large maximum enhancement ($\gamma_e/\gamma_{2H} = 4{,}300$) [82]. For proline, a polarization >700 was reported for ^{2}H using the Ox063 radical (see Sect. 3.4). This may become an interesting option for deuterated proteins.

Emsley and coworkers also reported surface enhanced NMR spectra for surface functionalized silica materials, where polarization is transferred from the protons of the solvent to the ^{13}C nuclei of functional groups at the surface, yielding at least a 50-fold signal enhancement [96].

As SS-DNP devices become commercially available we will most likely see widespread use across SS-NMR laboratories, and we may see results that render SS-DNP applicable for typical biological macromolecules.

3.1.1 Other Implementations of SS-DNP

There are now several implementations of gyrotrons, including a 260 GHz gyrotron oscillator (GYCOM, Russia) [94] and a 263 GHz gyrotron from Bruker (Germany),

with higher frequencies announced. Idehara et al. reported the design of a Terahertz (980 GHz) gyrotron suitable for high-field NMR experiments at 20 T and beyond [97].

Recent reports covered the implementation of several solid state DNP devices without MAS, including one by Feintuch et al. operating at 95 GHz [98], operable over a wide range of temperatures. A high-power pulsed DNP spectrometer, which was used to demonstrate higher DNP enhancements using pulsed compared to continuous wave electron excitation, was recently described by Hunter et al. [99]. Such pulsed EPR solutions are likely to open new avenues. Thurber et al. presented a low-power 264 GHz solution operating at 7–80 K [100], and a solution for submicron solid state NMR imaging [91].

3.2 O-DNP

O-DNP has only recently seen a renaissance after the early experiments by Hausser [37] and later by Müller-Warmuth [39]. The design of such spectrometers for true liquid-state DNP is dictated by the need to minimize heating, the unfortunate field dependency and the desire to obtain high-resolution spectra. There are two possible options: (1) to polarize at low field and transport the sample to higher (or in selected cases to lower) fields, an implementation that has found many applications; and (2) to conduct the entire experiment at one field strength. The second option is currently targeted towards mechanistic studies, although such implementations may have considerable potential for future applications, if some fundamental problems can be solved. High field implementations suffer from the need to build a probe that yields high quality factors for both NMR and EPR and from the low predicted enhancements, although recent results are increasingly encouraging.

3.2.1 Low to High Field Transfer O-DNP

In the 1980s, Dorn explored DNP enhancements for flowing liquids, first with an arrangement of nearby microwave and radiofrequency cells, operating at 9 GHz and 14 MHz, respectively, in a 0.35 T magnet [101]. Subsequently, he designed an apparatus that flows the sample from a 0.34 T microwave cavity into a 4.7 T NMR magnet (Fig. 8) [101]. The decisive advantage of this arrangement is the separation of the microwave excitation from the radiofrequency excitation/detection probe, thus allowing for an optimal arrangement at either site. Dorn used TEMPO radicals either in solution or immobilized on silica gel [101, 103]. The latter case he termed SLIT (solid–liquid intermolecular transfer) for which he observed impressive enhancements for small molecules in organic solvents. The key advantages of SLIT are the avoidance of contact shifts and line broadening owing to the presence of large concentrations of the radical, facile detection of scalar-dominated signals, good transfer efficiencies owing to slow relaxation, and suitability for a wide range of flow rates [103].

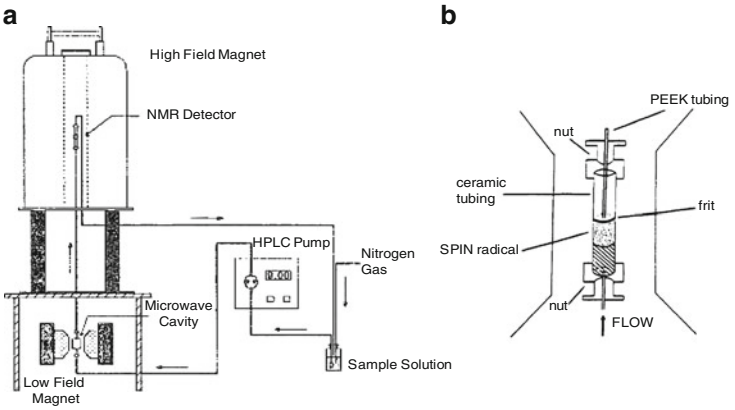

Fig. 8 (**a**) Dorn's O-DNP apparatus for continuous-flow online HPLC-DNP-NMR. (**b**) Diagram of the EPR flow cell employing TEMPO radicals immobilized on silica beads. [(**a**) kindly provided by Dorn; (**b**) reprinted from [102] with permission. Copyright 1994 American Chemical Society

For the case of dissolved radicals, Dorn found that much larger flow rates are required to obtain the optional enhancement, as a consequence of relaxation losses in the transfer [103]. Dorn derived a theoretical model to calculate the ultimate enhancements at low field [103], considering relaxation losses during the transfer, and achieved enhancements of −150 and −220 for benzene/dissolved TEMPO ^{1}H and ^{13}C, respectively. For chloroform/TEMPO he calculated extrapolated ^{1}H enhancements close to the dipolar limit of −330 and close to the scalar limit of 2,660 for ^{13}C for chlorinated carbons [104]. During flow these enhancements scale according to:

$$A_{\text{obs}} = A \cdot B_{\text{EPR}}/B_{\text{NMR}} \cdot (1 - E_{1a})E_{1b}E_{1c}, \tag{21}$$

where $A = \xi f s \frac{\gamma_e}{\gamma_n}$ (the "Overhauser enhancement"), B_{EPR} and B_{NMR} are the EPR and NMR field strengths, and $E_{1a,b,c} = \exp(-t_0/T_{1a,b,c})$ is the relaxation in regions a, b and c of the apparatus shown in Fig. 8a. For Dorn's spectrometer, signals were scaled by a field factor of 14.4. With the immobilized free radical, he obtained under flow conditions enhancement factors of −56 for chloroform and 1–10 for benzene (dipolar mechanism). For ^{13}C he observed a reduced enhancement owing to three-spin effects involving protons for benzene, and factors of 40–60 for chlorinated carbons that polarize via a scalar mechanism [103]. Dorn reported a strong dependence of the polarization mechanism on the radical concentration for dipolar-dominated enhancements, with compensating scalar and dipolar enhancements at lower radical concentrations.

Dorn also proposed to use DNP-enhanced NMR as a detector for continuous-flow online chromatography [102] and later described a recycled-flow spectrometer [103]. The drawback of this is, however, the large dead volume of the pump and tubing that considerably reduces the overall enhancement when compared to a smaller volume sample recorded in a conventional probe [103], as shown in

simulations of continuous flow NMR by Sudmeier et al. [105]. It would be worthwhile to reconsider the flow concept if the dead volumes could be further minimized.

The immobilized radical flow concept has recently been revisited by Lingwood et al. [106] to generate hyperpolarized water in the 0.35 T fringe field of a clinical 1.5 T whole-body MRI magnet, using an improved immobilized radical bound to Sepharose gel beads via polyelectrolyte linker arms. The system provides O-DNP enhancements approaching those of freely dissolved nitroxide radicals. This work reports a DNP signal enhancement factor of −15 in proton MRI images with respect to the unenhanced ^{1}H MRI signal of water at 1.5 T, reflecting an overall enhancement of −100 in the microwave cavity.

3.2.2 Shuttling DNP Spectrometer

A straightforward alternative to the continuous-flow concept is a shuttling solution, where either the sample or the probe is moved between magnets at two different field strengths. The concept of shuttling is quite old and was pioneered by Purcell and Pound in 1951 [107], who used it to examine the fate of a spin system upon field reversal. Several groups have implemented shuttling concepts since ([110–112], see [111] for a review on shuttling and field cycling).

Griesinger, Bennati and coworkers recently reported results from a concept shuttle spectrometer, polarizing at 9.7 GHz (0.23 T), on top of a 14.09 T magnet (600 MHz proton frequency). The maximum enhancement $I_{z,max}$ depends on the actual DNP enhancement (8) at low field (ϵ_{max}^{EPR}) and a field factor [56, 112]:

$$I_{z,max} = \epsilon_{max}^{EPR} I_0^{EPR} = \epsilon_{max}^{EPR} \left(B^{EPR}/B^{NMR}\right) I_0^{NMR} = \epsilon_{max}^{NMR} I_0^{NMR}. \tag{22}$$

The field ratio for the described implementation is ~41.4, i.e. a theoretical enhancement of −330 for a pure dipolar mechanism results, in the best case (for $\xi = f = s = 1$), in an overall NMR enhancement of ~8.

The apparatus shown in Fig. 9 [113] shuttles 0.9 or 0.46 mm inner diameter capillary samples within 140 ms between the magnet centres, which are 1.5 m apart. With a prototype version of this shuttle spectrometer an overall enhancement of −2.6 was observed for water doped with 5 mM TEMPONE-^{2}H,^{15}N [112], arising from an enhancement of −110 at low field. Much larger enhancements were observed for ^{13}C, +15 for $CHCl_3$ [112], in good agreement with large positive enhancements observed by Dorn. For 4 M urea, a negative enhancement with an ε_{eff} of -4 ± 1 was reported at radical concentrations of 25 mM [112]. Deuteration showed that three-spin effects (involving attached protons) play a minor role for urea. The low enhancement was therefore attributed to counteracting dipolar and scalar mechanisms.

In an improved setup (see [113] for a detailed description of the spectrometer and probe), relaxation-induced losses of hyperpolarization during the sample transfer were minimized by modifying the field profile so that the magnetic field never

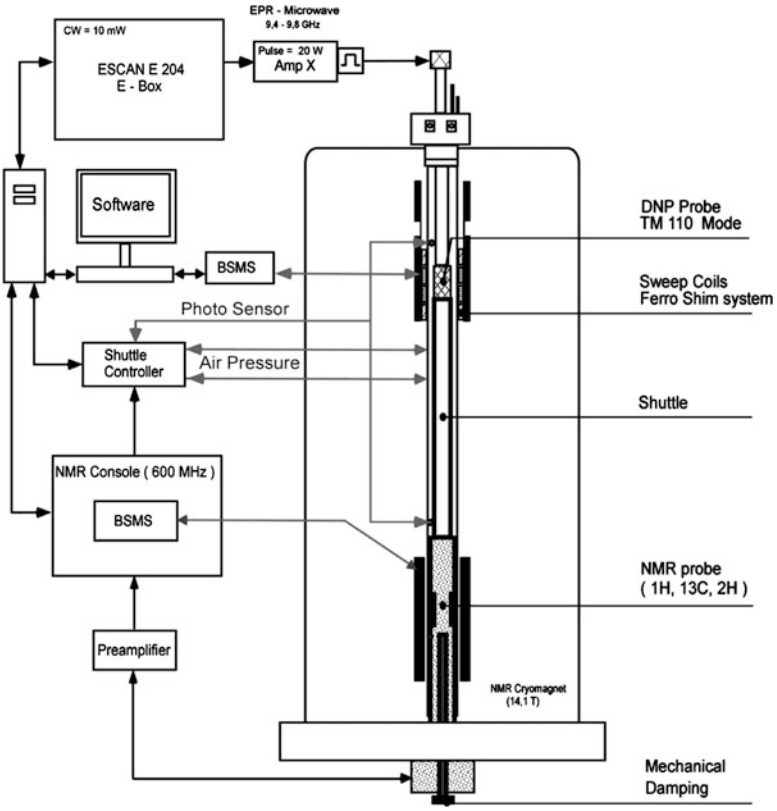

Fig. 9 O-DNP shuttling apparatus with an EPR spectrometer mounted on top of a 600 MHz magnet. An additional field plateau on top of the magnet is generated by a ferroshim system sitting in the stray field of the magnet. The EPR microwave cavity is connected to an EPR spectrometer. (Reproduced from [113] by permission of the PCCP Owner Societies)

dropped below the field strength of 0.34 T, at which hyperpolarization occurs (Fig. 10). An effective enhancement factor in the range of −1.4 to −2.8 was reported for the different protons of the D-glucose (10 mM $^{2}H,^{15}N$-TEMPONE solution in 99.8% D_2O with 5 mM DSS and 0.5 M D-glucose), reflecting relaxation losses for the glucose protons between 10 and 30%.

As pointed out by Griesinger and coworkers, losses during transfer associated with this arrangement are unfortunately still too large for protein applications [56]. Considering the field factor and relaxation losses during shuttling, any enhancement would be lost. To enable such a spectrometer for protein applications in solution therefore remains an unresolved challenge.

One major limitation of the shuttling implementations is, without doubt, the field factor between the EPR and NMR magnet. This could be reduced considerably with a 3.4 T (94 GHz) implementation of the polarizer, which would reduce the field

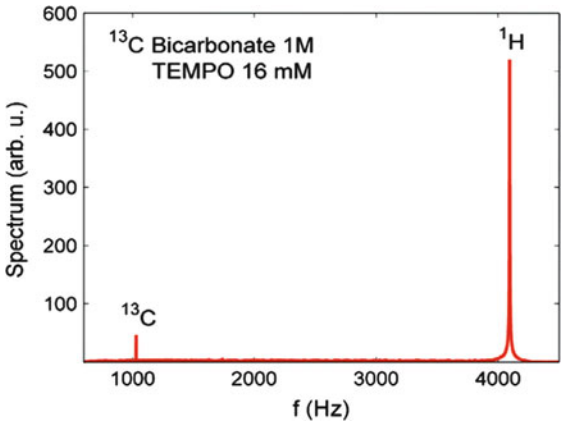

Fig. 10 Simultaneous measurement of proton and ^{13}C NMR signals of biscarbonate at 96 μT field using O-DNP [114]. Reprinted from [114], Copyright (2010), with permission from Elsevier

factor from ~41 to ~4.1. Such an arrangement would allow for larger enhancements, probably in the range of absolute values of ~10 for small molecules, considering smaller enhancements ε at larger field strengths. This is probably still not sufficient for protein applications, which would require much faster shuttling.

3.2.3 Stand-Alone O-DNP Polarizers

Many groups have implemented DNP spectrometers operating at microwave frequencies of ~9 and ~95 GHz, as the required hardware is readily and cheaply available. Many such systems are strictly add-on polarizers, some being used for MRI.

Münnemann described a mobile stand-alone polarizer using a Halbach permanent magnet operating at 0.30 T, corresponding to an electron frequency of ~9 GHz [115], designed to be used as a mobile DNP polarizer for clinical applications, but also to study enhancements at 3.2 MHz proton frequency in a relatively inhomogenous field. These authors compared different radicals: a trityl radical (TAM), TEMPOL (see Sect. 3.4) and a new spin-labelled cationic polyelectrolyte (poly(DADMAC)) with 4% nitroxide radical-bearing monomers and an average molecular weight of 490 kD. At high microwave powers, the DNP enhancement for water using poly(DADMAC) significantly exceeded those of TEMPOL. Enhancement values of −80 for poly (DADMAC), −60 for TEMPOL and −27 for the trityl radical were reported.

Han and coworkers presented several implementations of portable polarizers operating at 0.25 T/ 9.5 GHz microwave frequency [116]. In a first stand-alone solution using a fixed field electromagnet and alternatively a field-adjustable Halbach magnet, the authors reported an enhancement factor of −110 using the electromagnet for water and TEMPOL as a polarizer. For the more portable Halbach magnet, they achieved only a factor of −65, a consequence of a less optimal space-constrained microwave cavity.

3.2.4 DNP in the Earth's Field

It should be mentioned that μT earth field MRI is developing its own momentum. On the detection side, these experiments benefit from superconducting quantum interference devices (SQUID) [117], owing to the frequency independence of the SQUID devices. Earth field measurements were often combined with prepolarization in magnets with modest field strengths, benefiting from huge enhancements if combined with DNP, in particular if the polarization is carried out at higher field strengths (see [118] for a thorough theoretical treatment). Very low-field implementations represent an interesting theoretical challenge, as the Hamiltonian is not at all diagonal in product operator representations. For such low fields the hyperfine coupling term cannot be treated as a perturbation to the dominant Zeeman terms, but becomes strongly dominant.

A recent implementation by Halse, measuring in the Earth's field strength of 54 μT using nitroxide free radical microwave irradiation at 131.5 MHz in the presence of a 2.7 mT prepolarizing field was shown to yield an enhancement factor of −2,250 over thermal equilibrium [119]. Halse et al. also showed a ^{19}F–^{1}H COSY acquired of neat 2,2,2-trifluoroethanol in the Earth's magnetic field.

A more recent apparatus designed by Zotev et al. ([114], also see references included in this article) uses SQUID detectors and 96 μT, corresponding to the Larmor frequency of 4 kHz for protons and 1 kHz for ^{13}C. O-DNP was carried out with nitroxide radicals at 3.5–5.7 mT fields using radiofrequency irradiation at 120 MHz. The authors demonstrate applicability for imaging, but also for spectroscopy of ^{13}C-labelled metabolites such as sodium bicarbonate (Fig. 10), pyruvate, alanine and lactate. Enhancement factors or −95 for protons and −200 for ^{13}C, corresponding to thermal polarizations at 0.3 and 1.1 T field strengths, respectively, were reported. Such implementations could have significant impact for metabolic imaging, as an alternative to D-DNP, especially as NMR lines become very narrow at low fields, even for significantly inhomogeneous fields [117].

3.2.5 O-DNP Operating at a Single Field Strength for EPR and NMR

The challenge of O-DNP is undoubtedly to enable DNP in liquids at high magnetic fields, ideally at 600 MHz, or at least at 400 MHz proton frequencies. Such an implementation would eliminate the field factor, which lowers the enhancement for shuttle spectrometers. This requires a design of co-localized microwave and radiofrequency setup, ideally enabling high-resolution NMR spectra. One question is how much the enhancement drops at higher fields, further away from the $\omega_e \tau_c \ll 1$ condition. The design of such a DNP-NMR spectrometer has now been tackled by several groups, with implementations of up to 260 GHz. Although the overall challenge of detecting biological macromolecules in solution has not yet been met, there is some hope that this may become feasible in the future.

Recent fundamental work to identify the factors determining the efficiency of the polarization process (s, f and ξ) was primarily conducted by the groups of Bennati, Prisner, Kengens, Dupree and Han. Some of this has already been discussed in Sect. 2. A recent issue of *Physical Chemistry Chemical Physics* includes several articles examining O-DNP enhancements at 9.7, 94 and 260 GHz. Several studies show larger enhancements than expected from molecular dynamics simulations by Sezer [58]. These experiments along with the experimental implementations will be summarized next.

Bennati and coworkers examined experimentally the factors that determine efficient polarization at high fields, and compared enhancements at 9.7 and at 94 GHz [120]. For this purpose, two different DNP setups were used, both based on commercially available (Bruker) EPR spectrometers and ENDOR probes. For the 94 GHz DNP spectrometer, a 400 mW power upgrade was installed. The groups reported an O-DNP enhancement ε of −170 for water at 9.7 GHz (15 MHz proton frequency), using TEMPONE-D-^{15}N, the highest observed so far (Fig. 11a). However, at 94 GHz (140 MHz proton frequency) only an enhancement ε of −43 was achieved. These results showed that previous measurements by the same group yielding enhancements of −140 [121] were power-limited. A systematic study looking at the field dependence of the saturation factor, and measuring the temperature of the sample using different methods for different sample sizes, showed that saturation factors are near unity and coupling factors ξ are ~0.36 for radical

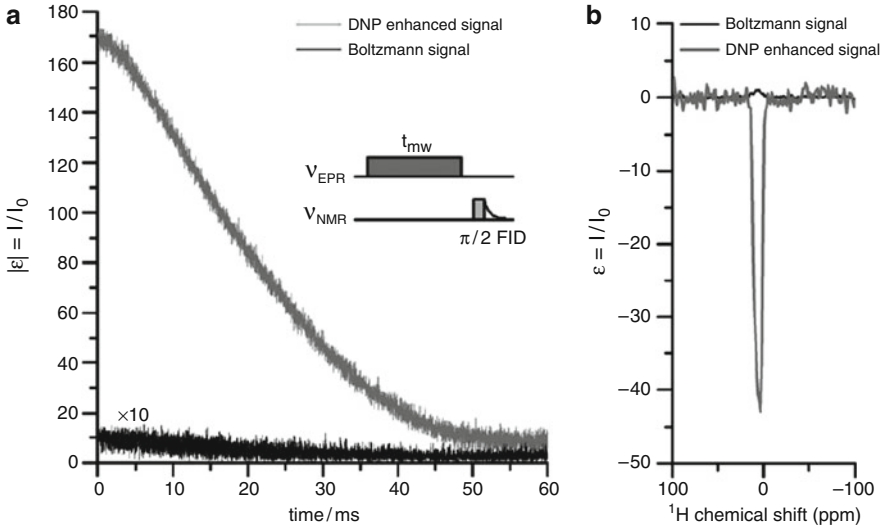

Fig. 11 O-DNP experiments by Bennati and coworkers. (**a**) Magnitude of the NMR free induction decay (FID) for 25 mM D-^{15}N-TEMPOL in water with and without microwave irradiation (9.7 GHz), showing a maximum enhancement ε of −170 for the first point of the FID. The Boltzmann signal required 4,096 scans whereas the DNP-enhanced signal was recorded within eight scans. (**b**) ^{1}H NMR spectra of water containing 25 mM D-^{15}N-TEMPONE at 94 GHz. (Reproduced from [45, 120] by permission of the PCCP Owner Societies)

concentrations of 5–10 mM and drop to 0.33 for 25–50 mM. These values were also found to be in good agreement with preceding NMRD measurements [54] and molecular dynamics (MD) calculations [58] but discard coupling factors determined by Armstrong et al. [55]. Saturation factors were ~0.8 when considering both lines and almost 1 when considering only one EPR line. At 94 GHz, the effective saturation factor s was estimated at 0.65, using a leakage f of 0.91, and a coupling factor ξ of 0.11 from MD measurements. It is therefore mainly the field dependence of ξ that is responsible for the lower enhancement at higher fields.

Kentgens and coworkers conducted a similar study using a DNP probe based on a novel double-resonance structure combining a single-mode microwave cavity resonating at 95 GHz with an intra-cavity radiofrequency coil operating at 95 GHz and 140 MHz [122]. These authors reported enhancements ε of -65 and extrapolated those to -94 in the centre of the resonator. These values are considerably higher than those reported by Bennati and coworkers; they are also higher than expected from MD calculations, even when some sample heating is considered.

A third implementation of high-field O-DNP was developed by Prisner and coworkers [123, 124]. In fact, they compared two high field implementations at 260 GHz and 400 MHz, using two different 260 GHz microwave sources, a high-power gyrotron microwave source (maximum power up to 20 W) and a solid-state microwave power source (maximum power 45 mW). Their setup uses a resonant microwave structure to separate electrical and magnetic field components for lossy solvents like water, and to increase the magnetic field strength at the sample (described in detail in [123]). The disadvantage of this setup is a very poor radiofrequency homogeneity, leading to broad NMR resonances, and the requirement for tiny capillary samples (0.03 mm inner diameter with few nanolitres of volume).

Prisner and coworkers started to use Fremy's salt as a radical, which exhibits a narrow EPR linewidth of less than 0.1 mT at 260 GHz [124] and yields much higher enhancements (-10 compared to -6) for ^{15}N-TEMPOL [122]. The gyrotron microwave source exhibited a striking improvement over that previously reported for the 45 mW source, yielding an enhancement value of -29 on water protons using Fremy's salt, compared to -10 previously reported for the 45 mW source (Fig. 12).

Denysenkov et al. discussed in detail the implications of this enhancement, which exceeds all expectations from preceding MD calculations [123]. The leakage factor was determined to be $f = 0.94$. The saturation factor s, which is more difficult to obtain owing to the short electron relaxation times T_{1e} and T_{2e}, was estimated computationally using Redfield's perturbation theory [125]. However, the variation of s within the possible window of T_{1e} of 100–400 ns cannot account for the high ε. For a coupling factor ξ of 0.072 estimated from MD calculations [58], a saturation factor of $s = 0.65$ was estimated, which is higher than expected from simulations. Such higher than theoretically expected enhancements can either be attributed to higher saturation factors or to incorrect temperature measurements, as suggested in [59].

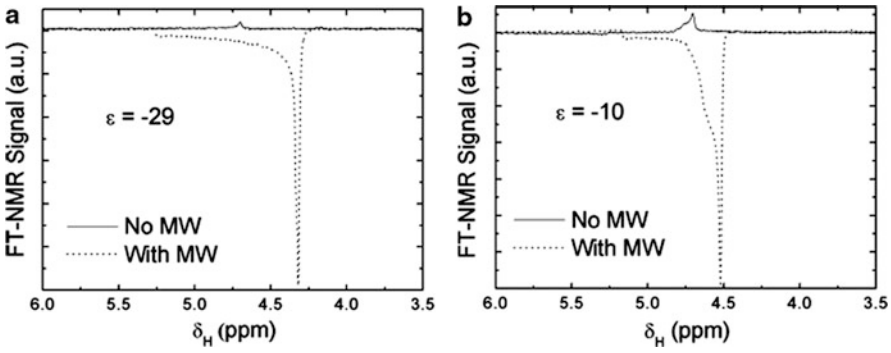

Fig. 12 Water ^{1}H NMR spectra reported by Prisner and coworkers, conducted at 9.2 T (260 Hz, 400 MHz); acquired with (*dots*) and without microwave pumping (*solid line*) on 40 mM aqueous Fremy's salt solutions using (**a**) a high power gyrotron, and (**b**) a low power solid-state microwave source. (Reproduced from [123] by permission of the PCCP Owner Societies)

Finally, Kryukov et al. designed an apparatus with a 100 W microwave amplifier operating at 94 GHz, using a modified Bruker ENDOR probe [126]. He examined TEMPOL in toluene, the only study looking at a non-aqueous solvent, and observed unexpectedly high enhancements of −43 for the methyl group and −50 for the ring protons [126]. A maximum enhancement was reported for a 20 mM concentration of TEMPO, similar to Bennati's results in water [120]. Again, enhancements were significantly greater than expected from extrapolation of early lower-field experiments, questioning preceding theoretical evaluations.

Direct observation of ^{13}C may be an option to overcome some of the limitations encountered for ^{1}H-DNP. This has already been demonstrated by Hausser at low field [37], and later by Loening et al. [127] at a magnetic field of 5 T (211 MHz for protons, 140 GHz for electrons), who reported an enhancement of −40 for tetrachloride (besides other heteronuclei). More recently, Lingwood et al. reported values of −265 for urea, +60 for *N*,*N*-dimethylformamide and −160 for pyruvate. Reese et al. reported effective high-field enhancements of +15 and −4 for chloroform and urea, respectively, using the earlier described shuttle spectrometer (see Fig. 13 for $CHCl_3$) [56]. The limitation for ^{13}C is the complex mechanism arising from competing scalar and dipolar effects, which may even compensate.

3.2.6 Applications of O-DNP

The overall picture arising from these implementations and applications suggest increased potential of O-DNP in solution. However, heating remains a serious problem that will limit applications, particularly for heat-sensitive biological macromolecules. The small sample sizes required in all implementations represent a serious practical obstacle. Large enhancements reported for higher fields suggest that a 94 GHz shuttle system may represent a worthwhile advantage over the existing 9.7 GHz implementation because the smaller field ratio will dominate over the

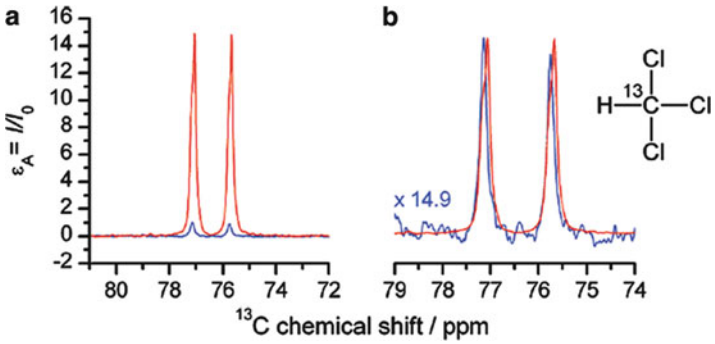

Fig. 13 ^{13}C (shuttle) DNP enhancement reported by Reese et al. [56] of ^{13}C-chloroform in water with 25 mM D-^{15}N-TEMPONE. The enhanced signals are compared with the Boltzmann polarization at 14 T. Reprinted with permission from [56]. Copyright 2009 American Chemical Society

somewhat reduced enhancement, predicting enhancements of at least 10 for protons. However, applications to biological macromolecules are currently limited by heating and shuttling times, which are still too long for protein relaxation times. So far, all measurements conducted at the same field strength for EPR and NMR suffer a from poor B_0 homogeneity, whereas shuttle spectrometers benefit from using a standard NMR probe to record high-resolution NMR spectra. Dorn's experiments pointed towards useful analytical applications of O-DNP, although hampered by the large amount of solvent required for the flow arrangement. If revisited, a much smaller dead volume and fast flow rate would have to be considered.

Several applications of O-DNP were suggested by Han and coworkers, who proposed hyperpolarized water as an MRI contrast agent, and applied this for the visualization of vortices in model reactors [51]. For in vivo MRI applications this approach is, however, limited by the relatively small enhancements for water, the requirement of using relatively toxic TEMPO radicals, and the fast relaxation of water (~1.5 s), leaving little time between the polarization, the administration of the polarized water and the MRI measurement. The same group also used DNP to study the dynamics of water at lipid vesicle surfaces [128], and more recently to study site-specific hydration translational dynamics in the core of a protein molten globule, using site-specific nitroxide spin labels [129]. The study shows that the translational dynamics of bound water in the nonpolar core of the molten globule of apomyoglobin is only four- to sixfold slower than that of bulk water. At this point such indirect measurements seem to be the only avenue towards the use of O-DNP in studies on biological macromolecules.

3.3 Dissolution and Temperature Jump DNP

Dissolution DNP and temperature jump DNP are two related concepts that share the common principle of carrying out the DNP enhancement at low temperatures,

followed by sample heating to prepare the sample in the liquid state for the acquisition of an NMR spectrum. Dissolution is achieved employing either hot solvent or laser heating. These implementations combine the power of carrying out NMR experiments in solution with the much larger DNP enhancements achievable at low temperatures.

3.3.1 Dissolution DNP

Dissolution DNP (also ex situ DNP), pioneered by Ardenkjær-Larsen [44], yields by far the largest overall enhancements of all implementations of DNP. This is achieved by polarizing in a lower field magnet (typically 3.4 T, microwave frequency 94 GHz) at 1.1–1.5 K, followed by rapidly melting and dissolving the hyperpolarized sample using hot solvent. The sample is then rapidly transferred into a conventional NMR magnet, to record the NMR spectrum ex situ at room temperature. This implementation combines a massive Boltzmann temperature enhancement of 200–250 with the actual DNP enhancement ε. The overall enhancement is defined by:

$$\epsilon' = \epsilon \cdot \frac{B_{\mathrm{DNP}}}{B_{\mathrm{NMR}}} \cdot \frac{T_{\mathrm{NMR}}}{T_{\mathrm{DNP}}}. \tag{23}$$

For a 11.75 T NMR system (500 MHz proton frequency) the B ratio amounts to 3.45. This is small compared to the huge temperature factor of ≈ 250. Even for modest DNP enhancements of $\approx$150, overall enhancements of $>$10,000 are obtained.

Figure 14 shows a scheme of the overall arrangement. This setup has found widespread use through the availability of a commercial implementation by Oxford

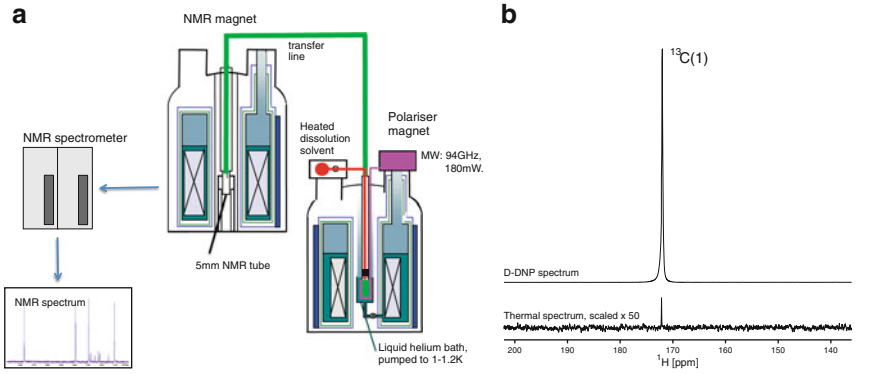

Fig. 14 (**a**) D-DNP setup. The sample is polarized at 1–1.3 K in the polarizer (shown on the *right*) and is subsequently transferred to the NMR magnet (*left*), where an NMR spectrum is recorded. Further details of this design can be found in [44]. (**b**) ^{13}C-NMR spectrum of ^{13}C(1)-pyruvate after D-DNP versus unpolarized, the latter vertically scaled by a factor of 50, showing the immense enhancement obtained by D-DNP

Instruments termed Hypersense™ [130], and due to the development towards clinical use by GE Healthcare [131]. There are, however, several alternative implementations, including a similar concept using a smaller He compartment [132], and a sophisticated solution using a two-centre magnet, designed by Köckenberger and coworkers [133].

The inevitable drawback of this implementation of DNP is the irreversible melting and dissolution of the sample, which limits the subsequent acquisition of NMR spectra to the life-time of the nuclear spins, i.e., the individual longitudinal relaxation times. While this seems to represent a major drawback, the huge enhancements observed for D-DNP may well compensate the loss of signal averaging, especially considering the availability of fast multidimensional acquisition schemes.

Experimental Conditions of D-DNP

As for SS-DNP, samples for D-DNP are prepared in a glassy matrix; crystalline (at least microcrystalline) samples do not yield any comparable polarization. Glasses can be readily prepared using mixtures of glycerol, DMSO, methanol and water. The Hypersense polarizer uses sample volumes of maximum 250 μL. A temperature of 1.1–1.3 K is reached by pumping on the He bath, regulating the He supply from the magnet's main He tank by a needle valve. The dissolution process is achieved using hot pressurized solvents, typically at 8–10 bar and ~200 °C, specific conditions depending on the dissolution solvent. After dissolution, samples are transferred into the NMR magnet through a tube by using gas pressure. Different dissolution solvents have been used, but mostly water and methanol, where the addition of methanol improves the sample flow and reduces bubble formation in the transfer process. To reach room temperature by dissolution it is usually necessary to use ~4 mL of solvent, of which only a fraction is transferred into the NMR tube (particularly when 5 mm NMR tubes holding 0.5 mL are used). Careful calibration of the solvent pressure and temperature guarantees a reasonably reproducible sample temperature after dissolution (±1 °C). The dissolution and transfer process each take 2–3 s, and this time frame restricts application to samples with sufficiently long relaxation times in the dissolution buffer. Hilty developed a sample injection device that enables significantly faster and more reliable sample injection in a time frame of ~600 ms [134]. With this arrangement, Hilty was able to record high quality spectra of glucose. Considering that spectra are recorded in a short time frame, pre-tuning and pre-shimming on standard samples yields reasonably good NMR spectra in unlocked mode.

The presence of the radical in the final sample (0.2–0.3 mM) affects relaxation times. Several methods have been described to remove the radical, e.g., filtration through a short anion-exchange column [44], radical quenching using a reducing agent [135], and precipitation under acidic conditions followed by mechanical filtration [131]. Removal of the radical is particularly important for in vivo applications because radicals are likely to be toxic, but also for analytical

applications of D-NMR, to minimize relaxation losses during the transfer from one magnet to the other.

D-DNP has had great success through the in vivo application of metabolic imaging, which holds great promise for clinical diagnostic applications. One of these in vivo applications is the detection of the fate of ^{13}C(1)-pyruvate in tumours, which characterizes the metabolic state of a tumour by the ratio of the metabolization products alanine and lactate [136, 137]. Another important in vivo application is the measurement of pH in vivo using hyperpolarized ^{13}C-labelled bicarbonate [138]; this can be used to image pathological processes associated with alterations in tissue pH, such as cancer, ischaemia and inflammation. The number of applications of metabolic imaging is growing quickly; the field deserves a separate review and will therefore not be covered here (see for example [139, 140]).

Polarization Mechanisms in D-NMR

Ardenkjær-Larsen first examined the polarization of ^{13}C-urea in glycerol with OX063 as a trityl radical (see Sect. 3.4) at 1.1 K. He observed a build-up constant τ of 4,900 s, while the T_{1n} of the ^{13}C signal was reported to be 28,200 s. For urea, a ^{13}C polarization of 42% was reached using15 mM OX063 at a temperature of 1.1 K. At 20 mM OX063, the polarization was reduced to 26%, and τ and T_{1n} were shortened to 2,755 and 15,800 s, respectively [44]. Based on microwave sweeps (polarization vs. microwave frequency curves) the ^{13}C polarization mechanism was attributed to thermal mixing, although a contribution by the SE could not be excluded. In the light of a rather lengthy polarization process, the SE seems to be more likely.

A more detailed examination of the polarization process of pyruvic acid at 1.1 K with 15 mM OX063Me [141] showed that T_{1e} is rather long at 0.91 s, and $T_{1n} \approx$ 12,000 s [for the pyruvic acid ^{13}C(1)]. T_{1n} also depends on the concentration of the radical ($T_{1n}^{-1} = 1.1 \cdot [\text{mmol/l}]^{-1} \cdot c + 82 \times 10^{-6}\text{s}^{-1}$). In the same work from the Ardenkjær-Larsen group, the effect of the addition of Gd^{3+} was examined. $GdCl3_3$ dramatically shortened T_{1e} at concentrations of 1 mM but not T_{1n}, and increased the achievable ^{13}C polarization, but not the build-up time.

Many aspects of the underlying mechanism remain enigmatic, and recent measurements show that the current level of understanding cannot even explain basic properties such as the field dependence of the polarization. For ^{13}C, a TM mechanism has been postulated considering that the homogenous width of the EPR signal is larger than the Larmor frequency ($\omega_{e1/2} = 63\text{MHz} > \omega_n = 35.88\text{MHz}$). Reynolds examined build-up curves and microwave sweeps for various nuclei, including ^{2}H, ^{31}P, ^{15}N, ^{13}C and ^{29}Si to determine the polarization mechanism in each case [142]. He measured the frequency separation of the opposite sign maxima and compared those to the Larmor frequencies of the nuclei (according to $\omega = \omega_e \pm \omega_n$ the separation should be $2\omega_n$ for the SE). All nuclei with ω_0 smaller than that of ^{13}C (35.96 MHz) were found to polarize via TM. This includes ^{15}N, ^{2}H and ^{29}Si. Only ^{31}P seems to polarize via a poorly resolved SE because its Larmor frequency

(58.875 MHz) is larger than the electron line half-width $\omega_{e1/2}$. Reynolds also observed a smaller secondary signal attributed to a double SE at a separation of about 147 MHz, attributed to a joint electron-heteronuclear-proton spin flip. Considering these frequency dependencies, it should be possible to polarize multiple nuclei with the same microwave frequency, which has in fact been demonstrated for ^{13}C and ^{15}N by Day et al. [143].

These findings raise the question whether the choice of a low temperature and a trityl radical enforces a TM mechanism. If this was the case it should be possible to identify conditions similar to those for CE in SS-DNP under which the effect could be optimized by using radicals with a suitable coupling between manifold of spins. Ardenkjær-Larsen and coworkers therefore explored trityl biradicals [144]. However, for a panel of biradicals the overall enhancement was lower than for monoradicals and was associated with a longer build-up time, although at lower optimal radical concentrations. No optimum trityl–trityl distance could be identified. Curiously, the ^{13}C T_{1n} was shortened for the biradicals, whereas T_{1e} was unaffected by radical type (and field strength).

However, both mono- and birdicals showed a doubling of the polarization when increasing the field from 3.35 to 4.64 T [141, 145]. Higher polarizations at higher field strength (5 T) were also reported by Jannin et al. [146]. This observation is clearly in disagreement with the expected B_0^{-1} dependence. Strangely, the enhanced polarization Gd^{3+} was not observed at the higher field of 4.64 T [141, 145]. These results make little sense in the light of existing theoretical models of either the SE or TM, and highlight a limited understanding of the polarization mechanism, even for simple systems.

Moreover, most biological applications of D-DNP use trityl radicals in pure pyruvic acid, void of any solvent addition. Compounds in smaller concentrations polarize at a much lower level, and this polarization level varies vastly between different substances. Some substances show little or no polarization despite a long T_1 (for example citrate, despite the long T_1 of its quaternary carbon) [147]. Polarizability strongly depends on the contact between the radical and the molecule to be polarized [147], and this contact is modulated by the solvent. Polarizability also depends fundamentally on the polarization matrix, in particular on efficient spin diffusion [43]. This is highlighted by studies showing optimal polarization for many small molecules in deuterated solvents, and in the presence of substances that improve spin diffusion by enhancing the network of ^{13}C atoms. As shown by Ludwig et al., higher enhancements can be achieved for many small molecules polarized in dilute solutions if $^{13}C(2)$-acetone is added to the polarization matrix as a co-polarization agent [66]. This effect was confirmed by Lumata et al., who observed faster polarization of pyruvate by adding ^{13}C-DMSO to the polarization matrix [67]. Similarly, solvent deuteration tends to reduce polarization times by reducing relaxation mechanisms that influence spin diffusion in the glassy sample matrix.

Moreover, for substances bearing methyl groups interference with quantum tunneling has been observed [70]. These arise from the sudden cooling, causing a skewed equilibrium for tunnel transitions in methyl quantum rotors.

Reestablishment of the equilibrium population is associated with changes in the spin state, through the influence of the exclusion principle on the space-spin symmetry of the molecular states. As a consequence, the signals of methyl ^{13}Cs may appear with different sign compared to the other resonances. As a consequence, the absolute intensity of the spectrum is not the same any more for microwave frequencies of $\omega_e - \omega_n$ versus $\omega_e + \omega_n$, because only the latter cause constructive interference of quantum rotor and DNP effects. It should be mentioned that quantum rotor mechanisms constitute a separate polarization mechanism with great potential [13, 15, 16].

Implementations of D-NMR

The immense enhancements ϵ' obtained for D-NMR have spurred several alternative implementations. A polarizer similar to the one described by Ardenkjær-Larsen has been designed and built by Comment et al. [132, 148]. He and his coworkers also explored polarization build-up at 1.2 K using TEMPO rather than trityl radicals [149], and found that a tight packing of spherical beads of 2–3 mm diameter, obtained by dripping the solution into liquid nitrogen, leads to higher polarizations, probably reflecting better microwave penetration into the sample. The highest polarization, of 14% or >15,000, reported by these authors was for 3 M acetate in a 9:1 mixture of D_2O and ethanol doped with 33 mM TEMPO. The main DNP mechanism was thought to be TM.

Köckenberger and coworkers designed a D-DNP polarizer using a dual-isocentre superconductive magnet with isocentres at 3.35 T and 9.4 T (400 MHz) separated by 85 cm [133], based on a magnet designed by Oxford Instruments. In this design, the polarizer system is placed on top, with the waveguides fed in through the top of the magnet. This system was designed to allow for sample transfer in the solid state, dissolving the sample only in very close proximity to the site where the NMR experiment is performed. The minimum magnetic field strength between the two isocentres is 0.2 T, thus avoid passage through very small or zero field. The system exhibits a transfer time and settling time of 2.9 s, about half of that achieved with conventional D-DNP systems. This system was characterized using an Ala–Gln dipeptide (Fig. 15) and a pentapeptide. Köckenberger and coworkers reported impressive results for these samples. Figure 15 shows the ^{1}H and ^{13}C spectra of the dipeptide, with enhancement factors for each ^{1}H resonance line for the dual centre magnet versus a stand-alone polarizer. An ϵ' of almost 3,000 was observed for C7 of Ala–Gln despite its rather short T_1 time constant of 700 ms.

Two-Dimensional Spectra Using D-DNP

The limited life-time of the polarization and the irreversibility of the dissolution process impose strict limitations on the types NMR of experiments that are feasible. Commonly, NMR experiments are recorded over longer time periods by averaging

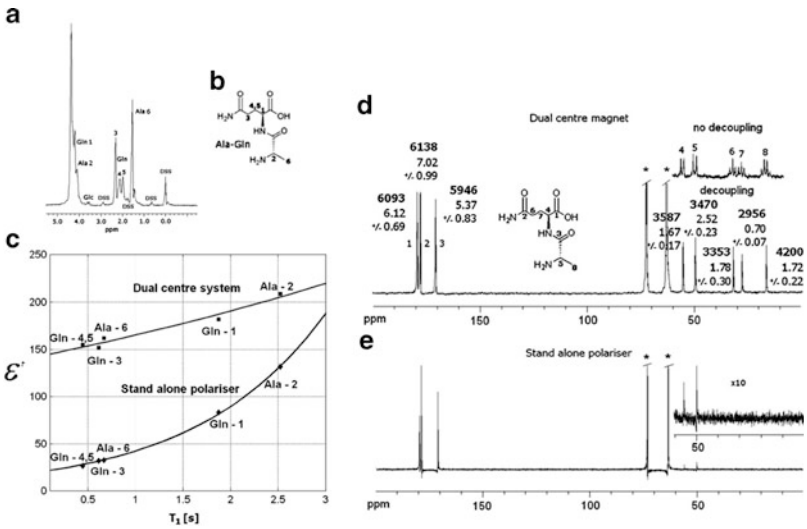

Fig. 15 (**a**) ^{1}H spectrum of the dipeptide Ala–Gln (**b**) after polarization at 3.4 T, shuttling in the solid state between isocentres of a dual-isocentre magnet and consecutive dissolution. (**c**) Comparison between enhancement factor ϵ' for the ^{1}H resonances of Ala–Gln after polarization in the dual-isocentre instrument versus using a stand-alone polarizer with pneumatic transfer. (**d**) Comparison of single scan ^{13}C spectra of a 0.5 mM solution of the Ala–Gln dipeptide (**b**) for the dual-isocentre DNP-NMR spectrometer versus a stand-alone polarizer. *Bold numbers* give the enhancement factor ϵ'. In addition, the T_1 relaxation time constants of the corresponding resonance lines are shown. (Reproduced from [133] by permission of the PCCP Owner Societies)

of larger numbers of scans. This is not possible with D-DNP because the NMR experiment has to be recorded within the life-time of the hyperpolarization.

To overcome this limitation, several authors have developed schemes to record two-dimensional spectra within the time frame imposed by the T_1 relaxation time constants of the molecules. Such experiments include gradient-encoded single-scan two-dimensional spectroscopy (ultrafast two-dimensional NMR) by Frydman and coworkers [150, 151] (Fig. 16a). Köckenberger used the ultrafast concept to implement a slice-selective single-scan proton COSY, demonstrated for a small peptide as shown in Fig. 16b [152]. Hilty used off-resonance decoupling to reconstruct a second dimension from a series of one-dimensional experiments [154], and later small flip angle excitation HMQC spectra [155]. Small flip angle single-run HMQCs were also used by Ludwig et al. [66], who combined this concept with nonlinear sampling to improve the resolution in such spectra (Fig. 16c, d).

Storage of Hyperpolarization

Considering the short T_1 relaxation time of some nuclei, it seems straightforward to explore longer-lived tags for D-DNP experiments. One of the options are acetyl

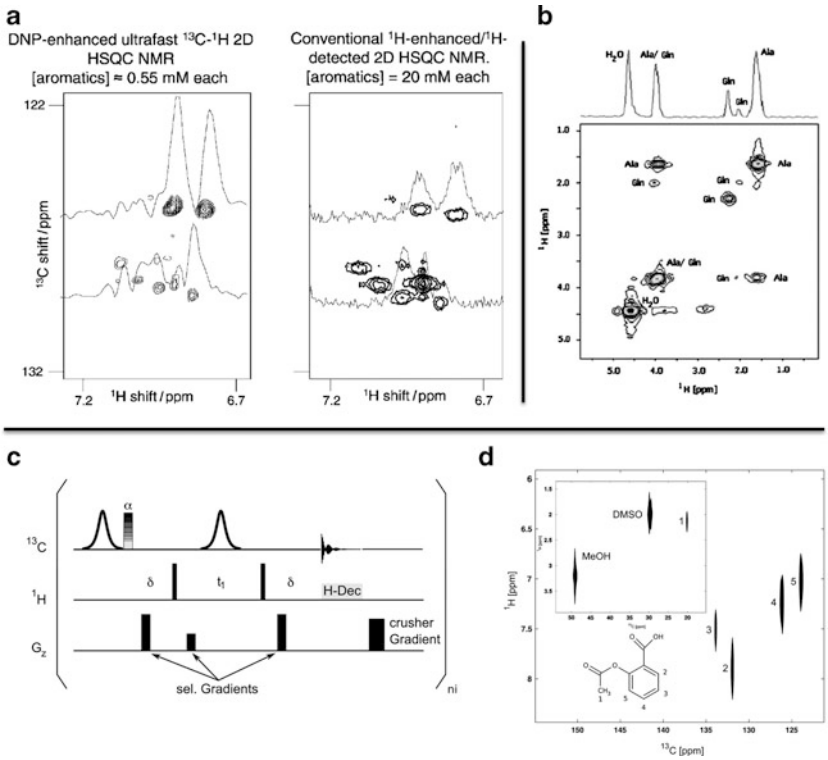

Fig. 16 Two-dimensional spectra from different authors, all using D-DNP and fast acquisition schemes. (**a**) ^{13}C-^{1}H-HSQC NMR spectra of a 1:1:1:1 mixture of *o*-, *m*-, and *p*-xylene and toluene, comparing a spectrum recorded by Frydman's ultrafast method (*left*) with a conventionally recorded spectrum (*right*) [150]. (Copyright Wiley-VCH. Reproduced with permission). (**b**) DNP enhanced proton COSY spectrum of 1.5 mM Ala–Gln at 9.4 T using an ultrafast COSY method by Köckenberger and coworkers. (Reproduced from [151] by permission of the PCCP Owner Societies). (**c**) 2D small flip angle ^{13}C-^{1}H-HMQC pulse sequence by Ludwig et al. [66, 153]. (**d**) 2D-HMQC spectrum of aspirin recorded in 30 s with 64 increments after 90 min of polarization at 1.3 K (kindly contributed by C. Ludwig)

tags, which can be attached to many small molecules near OH or NH_2 groups, and represent excellent substrates for D-DNP considering their relatively long T_1 relaxation time (>10 s at 11.7 T and 37 °C). The utility of acetyl tags for DNP was first realized by Wilson et al. [156] who used it to resolve a mixture of amino acids Gly, Ser, Val, Leu and Ala, for several small peptides and for *N*-acetylcysteine. Signal enhancements of up to 1,400-fold were reported for these molecules. It should be noted that this approach is limited to those amino acids that are sufficiently soluble before and after acetylation. Ludwig recently showed that ^{13}C-labelled acetyl tags produce a ^{13}C-^{13}C-NOE over a relatively long time that can be used to enhance ^{13}C signals after dissolution [153].

Bodenhausen and coworkers explored long-lived singlet spin states (LLS) to preserve hyperpolarization [157]. As shown by Levitt and coworkers, LLSs are delocalized on two or more coupled spins and have unusually long relaxation times because they are not affected by intramolecular dipole–dipole relaxation [158–160]. They can therefore be used to store magnetization, as demonstrated by Vasos et al. for the dipeptide Ala-Gly [157]. For this, the natural abundance dipeptide was polarized, the polarization on long-lived ^{13}CO carbons ($T_1 \approx 26$ s) in Gly was transferred via inverse INEPT to the Gly H^{α} protons, sustained over a period of time as long as $5T_{LLS}$, and finally transformed into detectable proton magnetization. The life-time of the LLS in Ala-Gly was reported to be ≈42 s.

Warren showed that in selected molecules such as 2,3-carbon-^{13}C–diacetyl with chemically equivalent nuclei, spin states with relatively long lifetimes exist that may be converted into detectable magnetization through a hydration reaction [161].

In principle, one of these options could be used to design tags, using either long-lived singlet spin states or simply groups with long T_1s, such as acetyl tags exhibiting T_1s of 20–30 s. For LLS, it would of course be preferable if the LLS could be generated in the polarizer to store polarization during the transfer process.

Applications of D-NMR

Despite the quasi "one-scan limitation" of D-NMR, the method has produced a multitude of interesting applications, including time-resolved real-time measurements of enzyme kinetics [162, 163], the analysis of biosynthetic pathways [164], the detection of low-populated reaction intermediates with hyperpolarized NMR [165], and ligand detected protein–ligand interactions [166]. Besides those biochemical applications, there is already a large base of literature on metabolic analyses and metabolic imaging (see for example [137, 139]). The existing work clearly demonstrates the applicability of D-DNP for chemical, biochemical and medical applications. A major drawback lies in the requirement of massive cooling, requiring ~1 L of liquid He per hour, indicating a need for more effective polarizers, possibly using smaller sample volumes.

3.3.2 In Situ Temperature-Jump DNP

Griffin and coworkers designed an alternative polarization scheme to enhance sensitivity in liquid-state NMR experiments of low-γ spins [167]. They cooled a sample to 90 K and polarized under CE conditions at 140 GHz using a biradical as polarizing agent, and subsequently cross-polarized from ^{1}H to low-γ nuclei, such as ^{13}C and ^{15}N. Instead of dissolving the sample irreversibly, the authors melted it rapidly employing an infrared laser pulse, before acquiring the spectrum in

solution. The theoretical enhancement in this case is $\epsilon' = \epsilon T_{obs}/T_{DNP}$. Enhancements of $\epsilon = 133\,(\epsilon' = 400)$ were reported for small molecules. The advantage of this concept lies in the fact that the sample is not irreversibly dissolved. It is therefore possible to perform signal averaging; freezing typically requires 60–90 s and the melting <1 s. Compared to D-DNP, the overall enhancements ϵ' are lower because the temperature factor is much smaller for temperature ratios of 300 K/100 K compared to 300 K/1.2 K. Temperature-jump DNP (TJ-DNP) could of course be extended to He cooling, although this would become rather impractical because 1.2 K requires an isolated He bath under reduced pressure, and cooling from 4 K to 1.2 K typically requires 5–10 min in common implementations of D-DNP polarizers. However, the combination of dissolution DNP with laser heating should be considered in order to reduce the volume of the dissolution solvent.

3.4 Polarizing Agents

Polarizing agents represent a core resource for DNP. They must exhibit a long lifetime of an unpaired electron, along with good solubility in the solvent of choice, i.e., in water for most biological applications. The most commonly used polarizing agents are now trityl (triarylmethyl) [44, 168–170] and nitroxide radicals. A thorough list of "older" radicals was compiled by Müller-Warmuth [39], who also characterized some for DNP via the OE mechanism.

Some common trityl radicals are shown in Fig. 17. TEMPO nitroxide radicals are frequently used for O-DNP, but also for SS-DNP. Common forms are 4-hydroxy-TEMPO (TEMPOL, also TEMPO) and 4-oxo-TEMPO (TEMPONE). Han showed that that deuteration and ^{15}N-labelling (^{2}H-^{15}N -TEMPONE) increases the saturation factor for O-DNP [51]. TEMPO-type radicals also facilitate the CE, in particular when used as biradicals. Griffin initially developed BTnE (bis-TEMPO-*n*-ethylene oxide) radicals with variable lengths of the linker [88], and later TOTAPOL (1-(TEMPO-4-oxy)-3-(TEMPO-4-amino)propan-2-ol) [89]. He also explored TEMPO-BDPA biradicals [171], and more recently rigid biradicals bTbk (bis-TEMPO-bisketal) [90]. Theoretical work showed that an orthogonal relative orientation of the electron g-tensors is a crucial requirement for obtaining high enhancement DNP factors [91]. Gafurov et al. explored bisnitroxide radicals for O-DNP but found no advantage over monoradicals [172].

For dissolution DNP polarizing via the SE or TM, radicals with narrow lines are required. This is the case for highly symmetrical trityl radicals, which were originally developed by Nycomed as MRI contrast agents [44, 168, 169]. The most commonly used radical of this kind is OX063 (tris{8-carboxyl-2,2,6,6-tetra[2-(1-hydroxyethyl)]-benzo(1,2-d:4,5-d′)bis(1,3)dithiole-4-yl}methyl sodium salt), shown in Fig. 17. Ardenkjær-Larsen explored trityl biradicals and found lower concentrations for optimal polarization, but at the price of much longer build-up times. Pons explored chlorinated versions of trityl radicals (see

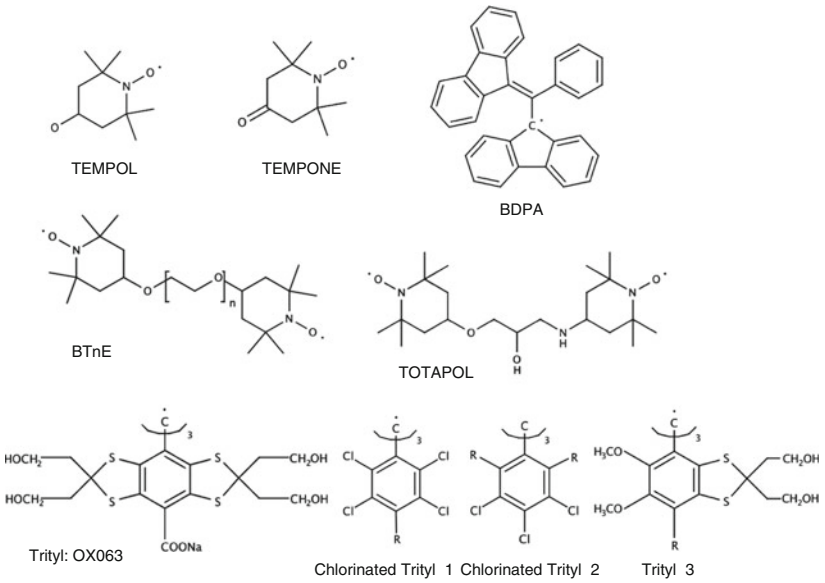

Fig. 17 Chemical structures of radicals used for DNP experiments

Fig. 17), which are also suitable for D-DNP but seem to alter the polarization mechanism, showing marked differences between neutral and anionic forms of the radical [173]. Density functional theory (DFT) calculations support the hypothesis that in these radicals polarization is transferred from the unpaired electron to chlorine nuclei, and from these to carbon by spin diffusion [174].

Recently, Stephan presented a tunable structure that allows easy access to an array of trityl radicals possessing modular surface functional groups (trityl 3 in Fig. 17) [175]. While these radicals are less symmetrical they showed comparable enhancements for small molecules (Stephan and Günther, unpublished results from this laboratory).

Corzilius recently reported high-spin transition metal compounds (Mn^{2+} and Gd^{3+}) as polarizing agents. When the EPR linewidth is narrow and there is no spectral dilution by strong hyperfine coupling to the metal nucleus, DNP performance was shown to be comparable to that obtained with trityl radicals. This finding puts the reports on larger polarizations employing Gd^{3+} into a different perspective [143, 145], and probably requires reconsideration of the polarization mechanism in the presence of Gd^{3+}.

Recently, Dollmann et al. introduced potentially biocompatible spin-labelled heparins, which have remarkable features for O-DNP [176]. For these compounds, the off-resonant EPR hyperfine lines contribute to the total saturation, even in the absence of Heisenberg spin exchange (HSE) and electron spin–nuclear spin relaxation (T_{1ne}). Alternatively spin-labelled hydrogels were proposed [177], which may have unique advantages for shuttle DNP experiments

owing to the prolonged lifetime of the hyperpolarization. Münnemann also explored a spin-labelled cationic polyelectrolyte poly(DADMAC) [a copolymer of poly(diallyldi-methyl-ammonium chloride with 4% nitroxide radical-bearing monomers], as mentioned earlier [115].

4 Conclusions

Without doubt, DNP applications have started to open new avenues for increasing the range of NMR applications. However, there is no universal solution that provides large enhancements for a broad range of NMR application. The only implementation directly applicable to biological macromolecules is SS-DNP, although enhancements for proteins seem to be smaller than for small molecules and further work is needed to enable wide-spread applications for biological macromolecules. This is, however, clearly facilitated by substantial groundwork and the availability of commercial implementations.

D-DNP has enormous potential for medical applications using metabolic imaging, and is likely to provide exciting new solutions for bioanalytical NMR. However, the requirement for He cooling considerably increases the operational costs of the spectrometer, and the requirement for sample freezing, dissolution and transfer limits applications. Nevertheless, driven by the immense enhancements for some molecules, a range of interesting solutions has already been proposed. D-DNP also benefits from a commercially available polarizer and emerging solution that speed up sample dissolution and transfer. For polarizations carried out in the solid state, the theoretical description remains incomplete.

O-DNP, the only DNP-method carrying out polarizations in liquids, has benefited from a series of mechanistic studies to characterize the polarization parameters. From this groundwork it is becoming increasingly clear that considerable enhancements are feasible, although sample heating remains a significant problem. Shuttling or flow solutions present an interesting compromise but are limited to modest enhancements, whereas polarization and acquisition at higher field require further optimizations, implementing significant cooling and polarization cells enabling higher resolutions on NMR spectra.

Although this review is mainly focused on DNP, there are several parallel developments generating hyperpolarization sources other than unpaired electrons, some of which were mentioned in the “Introduction”. Some methods yield 100% theoretical polarization, although requiring a different set of compromises to realize these enhancements for practical samples.

Without doubt, hyperpolarization methods have entered the arena of biomedical NMR, although more work is needed to provide practical implementations. Considering that the first DNP experiment was carried out almost half a century ago, it is astonishing that many polarization mechanisms remain poorly understood, leaving exiting opportunities for further work.

Acknowledgments I would like to thank Marina Bennati and Thomas Prisner for helpful discussions. I would like to thank Christian Ludwig for providing additional data for Fig. 16d. I also thank Christian Ludwig and Rafael Brüschweiler for critical proof reading.

References

1. Abragam A (1961) Principles of nuclear magnetism. Oxford University Press, London
2. Jeffries CD (1964) Ann Rev Nucl Sci 14:101
3. Bouchiat M, Carver T, Varnum C (1960) Phys Rev Lett 5:373
4. Eisenschmid TC, Kirss RU, Deutsch PP, Hommeltoft SI, Eisenberg R, Bargon J, Lawler RG, Balch AL (1987) J Am Chem Soc 109:8089
5. Bowers CR, Weitekamp DP (1986) Phys Rev Lett 57:2645
6. Bargon J, Fischer H, Johnsen U (1967) Z Naturforsch A 22:1551
7. Ward HR, Lawler RG (1967) J Am Chem Soc 89:5518
8. Closs GL (1969) J Am Chem Soc 91:4552
9. Kaptein R, Dijkstra K, Nicolay K (1978) Nature 274:293
10. Adams R, Aguilar J, Atkinson K, Cowley M, Elliott P, Duckett S, Green G, Khazal I, Lopez-Serrano J, Williamson D (2009) Science 323:1708
11. Haupt J (1972) Phys Lett A A 38:389
12. Horsewill AJ (1999) Prog Nucl Magn Reson Spectrosc 35:359
13. Ludwig C, Saunders M, Marin-Montesinos I, Günther UL (2010) Proc Natl Acad Sci USA 107:10799
14. Tomaselli M, Meier U, Meier BH (2004) J Chem Phys 120:4051
15. Tomaselli M, Knecht DW, Holleman I, Meijer G, Meier BH (2000) J Chem Phys 113:5141
16. Tomaselli M, Meier BH (2001) J Chem Phys 115:11017
17. Bifone A, Song YQ, Seydoux R, Taylor RE, Goodson BM, Pietrass T, Budinger TF, Navon G, Pines A (1996) Proc Natl Acad Sci USA 93:12932
18. Lampel G (1968) Phys Rev Lett 20:491
19. Albert MS, Cates GD, Driehuys B, Happer W, Saam B, Springer CS Jr, Wishnia A (1994) Nature 370:199
20. Navon G, Song Y-Q, Rõõm T, Appelt S, Taylor R, Pines A (1996) Science 271:1848
21. Overhauser AW (1953) Phys Rev 92:411
22. Carver TR, Slichter CP (1953) Phys Rev 92:212
23. Carver TR, Slichter CP (1956) Phys Rev 102:975
24. Pound RV (1950) Phys Rev 79:685
25. Abragam A (1955) Phys Rev 98:1729
26. Jeffries CD (1957) Phys Rev 106:164
27. Borghini M (1968) Phys Rev Lett 20:419
28. Borghini M, Scheffler K (1971) Phys Rev Lett 26:1362
29. Abragam A, Proctor W (1958) C R Hebd Seances Acad Sci 246:2253
30. Kessenikh A, Lushchinov V, Manekov A, Taran Y (1963) Sov Phys Solid State 5:321
31. Kessenikh A, Manenkov A, Lyatnitskii G (1964) Sov Phys Solid State 6:641
32. Hwang CF, Hill D (1967) Phys Rev Lett 18:110
33. Hwang CF, Hill DA (1967) Phys Rev Lett 19:1011
34. Byvik CE, Wollan DS (1974) Phys Rev B 10:791
35. Wollan DS (1976) Phys Rev B 13:3686
36. Wind RA, Duijvestijn MJ, van der Lugt C, Manenschijn A, Vriend J (1985) Prog Nucl Magn Reson Spectrosc 17:33
37. Hausser K, Stehlik D (1968) Adv Magn Reson 3:79
38. Hall D, Maus D, Gerfen G, Inati S, Becerra L, Dahlquist F, Griffin R (1997) Science 276:930

39. Müller-Warmuth W, Meise-Gresch K (1983) Adv Magnn Reson 11:1
40. Bennati M, Tkach I, Türke M-T (2011) Electron Paramagn Reson 22:155
41. Abragam A, Goldman M (1978) Rep Prog Phys 41:395
42. Maly T, Debelouchina GT, Bajaj VS, Hu KN, Joo CG, Mak-Jurkauskas ML, Sirigiri JR, van der Wel PC, Herzfeld J, Temkin RJ, Griffin RG (2008) J Chem Phys 128:052211
43. Hovav Y, Feintuch A, Vega S (2011) J Chem Phys 134:074509
44. Ardenkjaer-Larsen JH, Fridlund B, Gram A, Hansson G, Hansson L, Lerche MH, Servin R, Thaning M, Golman K (2003) Proc Natl Acad Sci 100:10158
45. Slichter CP (2010) Phys Chem Chem Phys 12:5741
46. Denninger G, Stocklein W, Dormann E, Schwoerer M (1984) Chem Phys Lett 107:222
47. Stocklein W, Seidel H, Singel D, Kendrick R, Yannoni C (1987) Chem Phys Lett 141:277
48. Wind RA, Lock H, Mehring M (1987) Chem Phys Lett 141:283
49. Solomon I (1955) Phys Rev Lett 99:959
50. Bates R Jr, Drozdoski W (1977) J Chem Phys 67:4038
51. Armstrong B, Han S (2007) J Chem Phys 127:104508
52. Abragam A, Pound R (1953) Phys Rev 92:943
53. Hwang LP, Freed JH (1975) J Chem Phys 63:4017
54. Bennati M, Luchinat C, Parigi G, Türke M (2010) Phys Chem Chem Phys 12:5902
55. Armstrong BD, Han S (2009) J Am Chem Soc 131:4641
56. Reese M, Türke MT, Tkach I, Parigi G, Luchinat C, Marquardsen T, Tavernier A, Hofer P, Engelke F, Griesinger C, Bennati M (2009) J Am Chem Soc 131:15086
57. Lingwood M, Han S (2009) J Magn Reson 201:137
58. Sezer D, Prandolini MJ, Prisner TF (2009) Phys Chem Chem Phys 11:6626
59. Kryukov EV, Pike KJ, Tam TKY, Newton ME, Smith ME, Dupree R (2011) Phys Chem Chem Phys 13:4372
60. Jeffries CD (1960) Phys Rev 117:1056
61. Wenckebach WT (2008) Appl Magn Reson 34:227
62. Henstra A, Wenckebach WT (2008) Mol Phys 106:859
63. Jeschke G, Schweiger A (1996) Mol Phys 88(2):335
64. Henstra A, Dirksen P, Schmidt J, Wenckebach WT (1988) J Magn Reson 77:389
65. Wind R, Lock H (1990) Adv Magn Opt Reson 15:51
66. Ludwig C, Marin-Montesinos I, Saunders MG, Günther UL (2010) J Am Chem Soc 132:2508
67. Lumata L, Kovacs Z, Malloy C, Sherry AD, Merritt M (2011) Phys Med Biol 56:N85
68. Bloembergen N (1949) Physica 15:3386
69. Dementyev AE, Cory DG, Ramanathan C (2008) Phys Rev Lett 100:127601
70. Saunders MG, Ludwig C, Günther UL (2008) J Am Chem Soc 130:6914
71. Abragam A, Borghini M (1964) In: Gorter C (ed) Progress in low temperature physics, vol IV. North-Holland Publishing Company, Amsterdam
72. Goldman M (1970) Spin temperature and nuclear magnetic resonance in solids. Oxford University Press, Oxford
73. Goertz S (2004) Nucl Instrum Methods Phys Res A 526:28
74. Radtke E, Reicherz G, Schiemann M (2008) Appl Magn Reson 34:461
75. Wind R, Li L, Lock H, Maciel G (1988) J Magn Reson 79:577
76. Henstra A, Dirksen P, Wenckebach WT (1988) Phys Lett A 134:134
77. Henstra A, Lin T, Schmidt J, Wenckebach W (1990) Chem Phys Lett 165:6
78. Weis V, Bennati M, Rosay M, Griffin RG (2000) J Chem Phys 113:6795
79. Morley GW, van Tol J, Ardavan A, Porfyrakis K, Zhang J, Briggs GA (2007) Phys Rev Lett 98:220501
80. Bajaj V, Farrar C, Hornstein M, Mastovsky I, Vieregg J, Bryant J, Elena B, Kreischer K, Temkin R, Griffin R (2003) J Magn Reson 160:85
81. Bajaj VS, Hornstein MK, Kreischer KE, Sirigiri JR, Woskov PP, Mak-Jurkauskas ML, Herzfeld J, Temkin RJ, Griffin RG (2007) J Magn Reson 189:251

82. Maly T, Andreas LB, Smith AA, Griffin RG (2010) Phys Chem Chem Phys 12:5872
83. Wind R, Anthonio F, Duijvestijn M, Smidt J, Trommel J, de Vette G (1983) J Magn Reson 52:424
84. Afeworki M, McKay RA, Schaefer J (1992) Macromolecules 25:4084
85. Becerra LR, Gerfen GJ, Temkin RJ, Singel DJ, Griffin RG (1993) Phys Rev Lett 71:3561
86. Becerra L, Gerfen G, Bellew B, Bryant J, Hall D, Inati S, Weber R, Un S, Prisner T, McDermott A (1995) J Magn Reson Series A 117:28
87. Hu KN, Yu H, Swager TM, Griffin RG (2004) J Am Chem Soc 126:10844
88. Song C, Hu KN, Joo CG, Swager TM, Griffin RG (2006) J Am Chem Soc 128:11385
89. Matsuki Y, Maly T, Ouari O, Karoui H, Le Moigne F, Rizzato E, Lyubenova S, Herzfeld J, Prisner T, Tordo P, Griffin RG (2009) Angew Chem Int Ed Engl 48:4996
90. Ysacco C, Rizzato E, Virolleaud M-A, Karoui H, Rockenbauer A, Le Moigne F, Siri D, Ouari O, Griffin RG, Tordo P (2010) Phys Chem Chem Phys 12:5841
91. Thurber KR, Tycko R (2010) Phys Chem Chem Phys 12:5779
92. Barnes AB, Corzilius B, Mak-Jurkauskas ML, Andreas LB, Bajaj VS, Matsuki Y, Belenky ML, Lugtenburg J, Sirigiri JR, Temkin RJ, Herzfeld J, Griffin RG (2010) Phys Chem Chem Phys 12:5861
93. Debelouchina GT, Bayro MJ, Van Der Wel PCA, Caporini MA, Barnes AB, Rosay M, Maas WE, Griffin RG (2010) Phys Chem Chem Phys 12:5911
94. Akbey U, Franks WT, Linden A, Lange S, Griffin RG, van Rossum BJ, Oschkinat H (2010) Angew Chem Int Ed Engl 49:7803
95. Maly T, Miller AF, Griffin RG (2010) Chemphyschem 11:999
96. Lesage A, Lelli M, Gajan D, Caporini MA, Vitzthum V, Mieville P, Alauzun J, Roussey A, Thieuleux C, Mehdi A, Bodenhausen G, Coperet C, Emsley L (2010) J Am Chem Soc 132:15459
97. Idehara T, Saito T, Ogawa I, Mitsudo S, Tatematsu Y, Agusu L, Mori H, Kobayashi S (2008) Appl Magn Reson 34:265
98. Feintuch A, Shimon D, Hovav Y, Banerjee D, Kaminker I, Lipkin Y, Zibzener K, Epel B, Vega S, Goldfarb D (2011) J Magn Reson 209:136
99. Hunter RI, Cruickshank PAS, Bolton DR, Riedi PC, Smith GM (2010) Phys Chem Chem Phys 12:5752
100. Thurber KR, Yau WM, Tycko R (2010) J Magn Reson 204:303
101. Dorn HC, Wang J, Allen L, Sweeney D, Glass T (1988) J Magn Reson 79:404
102. Stevenson S, Dorn HC (1994) Anal Chem 66:2993
103. Stevenson S, Glass T, Dorn H (1998) Anal Chem 70:2623
104. Dorn H, Gitti R, Tsai K, Glass T (1989) Chem Phys Lett 155:227
105. Sudmeier JL, Günther UL, Albert K, Bachovchin WW (1996) J Magn Reson A 118:145
106. Lingwood M, Siaw T, Sailasuta N, Ross B, Bhattacharya P, Han S (2010) J Magn Reson 205:247
107. Purcell EM, Pound RV (1951) Phys Rev 81:279
108. Redfield AG (2003) Magn Reson Chem 41:753
109. Grosse S, Gubaydullin F, Scheelken H, Vieth HM, Yurkovskaya AV (1999) Appl Magn Reson 17:211
110. Victor K, Kavolius V, Bryant R (2004) J Magn Reson 171:253
111. Noack F (1986) Prog Nucl Magn Reson Spectrosc 18:171
112. Reese M, Lennartz D, Marquardsen T, Höfer P, Tavernier A, Carl P, Schippmann T, Bennati M, Carlomagno T, Engelke F, Griesinger C (2008) Appl Magn Reson 34:301
113. Krahn A, Lottmann P, Marquardsen T, Tavernier A, Türke M, Reese M, Leonov A, Bennati M, Hoefer P, Engelke F (2010) Phys Chem Chem Phys 12:5830
114. Zotev VS, Owens T, Matlashov AN, Savukov IM, Gomez JJ, Espy MA (2010) J Magn Reson 207:78
115. Münnemann K, Bauer C, Schmiedeskam J, Spiess H, Schreiber W, Hiderberger D (2008) Appl Magn Reson 34:321

116. Armstrong B, Lingwood M, McCarney E, Brown E, Blümler P, Han S (2008) J Magn Reson 191:273
117. McDermott R (2002) Science 295:2247
118. Guiberteau T, Grucker D (1996) J Magn Reson Series B 110:47
119. Halse ME, Callaghan PT (2008) J Magn Reson 195:162
120. Türke MT, Tkach I, Reese M, Höfer P, Bennati M (2010) Phys Chem Chem Phys 12:5893
121. Höfer P, Parigi G, Luchinat C, Carl P, Guthausen G, Reese M, Carlomagno T, Griesinger C, Bennati M (2008) J Am Chem Soc 130:3254
122. Villanueva-Garibay JA, Annino G, Van Bentum PJM, Kentgens APM (2010) Phys Chem Chem Phys 12:5846
123. Denysenkov V, Prandolini MJ, Gafurov M, Sezer D, Endeward B, Prisner TF (2010) Phys Chem Chem Phys 12:5786
124. Prandolini MJ, Denysenkov VP, Gafurov M, Endeward B, Prisner TF (2009) J Am Chem Soc 131:6090
125. Sezer D, Gafurov M, Prandolini MJ, Denysenkov VP, Prisner T (2009) Phys Chem Chem Phys 11:6638
126. Kryukov EV, Newton ME, Pike KJ, Bolton DR, Kowalczyk RM, Howes AP, Smith ME, Dupree R (2010) Phys Chem Chem Phys 12:5757
127. Loening N, Rosay M, Weis V, Griffin R (2002) J Am Chem Soc 124:8808
128. Kausik R, Han S (2009) J Am Chem Soc 131:18254
129. Armstrong BD, Choi J, Lopez C, Wesener DA, Hubbell W, Cavagnero S, Han S (2011) J Am Chem Soc 133:5987
130. Sowerby A (2005) Chem Ind:21
131. Ardenkjaer-Larsen JH, Leach AM, Clarke N, Urbahn J, Anderson D, Skloss TW (2011) NMR Biomed 24:927–932
132. Comment A, van den Brandt B, Uffmann K, Kurdzesau F, Jannin S, Konter JA, Hautle P, Wenckebach WT, Gruetter R, Van Der Klink J (2007) Concepts Magn Reson 31B:225
133. Leggett J, Hunter R, Granwehr J, Panek R, Perez-Linde AJ, Horsewill AJ, McMaster J, Smith G, Kockenberger W (2010) Phys Chem Chem Phys 12:5883
134. Bowen S, Hilty C (2010) Phys Chem Chem Phys 12:5766
135. Liu Y, Villamena FA, Rockenbauer A, Rockenbauer A, Zweier J (2010) Chem Commun (Camb) 46:628
136. Day SE, Kettunen MI, Gallagher FA, Hu DE, Lerche M, Wolber J, Golman K, Ardenkjaer-Larsen JH, Brindle KM (2007) Nat Med 13:1382
137. Brindle K (2008) Nat Rev Cancer 8:94
138. Gallagher FA, Kettunen MI, Day SE, Hu D-E, Ardenkjaer-Larsen JH, Zandt RIt, Jensen PR, Karlsson M, Golman K, Lerche MH, Brindle KM (2008) Nature 453:940
139. Nelson S, Vigneron D, Kurhanewicz J, Chen A, Bok R, Hurd D (2008) Appl Magn Reson 34:533
140. Golman K, Zandt RI, Lerche M, Pehrson R, Ardenkjaer-Larsen JH (2006) Cancer Res 66:10855
141. Ardenkjaer-Larsen J, Macholl S, Johannesson H (2008) Appl Magn Reson 34:509
142. Reynolds S, Patel H (2008) Appl Magn Reson 34:495
143. Day IJ, Mitchell JC, Snowden MJ, Davis AL (2007) Magn Reson Chem 45:1018
144. Macholl S, Johannesson H, Ardenkjaer-Larsen JH (2010) Phys Chem Chem Phys 12:5804
145. Johannesson H, Macholl S, Ardenkjaer-Larsen JH (2009) J Magn Reson 197:167
146. Jannin S, Comment A, Kurdzesau F, Konter JA, Hautle P, van den Brandt B, van der Klink JJ (2008) J Chem Phys 128:241102
147. Emwas A-H, Saunders M, Ludwig C, Günther U (2008) Appl Magn Reson 34:483
148. Comment A, Rentsch J, Kurdzesau F, Jannin S, Uffmann K, van Heeswijk RB, Hautle P, Konter JA, van den Brandt B, van der Klink JJ (2008) J Magn Reson 194:152
149. Kurdzesau F, van den Brandt B, Comment A, Hautle P, Jannin S, Van Der Klink J, Konter J (2008) J Phys D: Appl Phys 41:155506

150. Mishkovsky M, Frydman L (2008) Phys Chem Chem Phys 9:2340
151. Frydman L, Blazina D (2007) Nat Phys 3:415
152. Panek R, Granwehr J, Leggett J, Kockenberger W (2010) Phys Chem Chem Phys 12:5771
153. Ludwig C, Marin-Montesinos I, Saunders MG, Emwas AH, Pikramenou Z, Hammond SP, Günther UL (2010) Phys Chem Chem Phys 12:5868
154. Bowen S, Zeng H, Hilty C (2008) Anal Chem 80:5794
155. Zeng H, Bowen S, Hilty C (2009) J Magn Reson 199:159
156. Wilson D, Hurd R, Keshari K et al. (2009) Proc Natl Acad Sci USA 106:5503
157. Vasos PR, Comment A, Sarkar R, Ahuja P, Jannin S, Ansermet JP, Konter JA, Hautle P, van den Brandt B, Bodenhausen G (2009) Proc Natl Acad Sci USA 106:18469
158. Pileio G, Carravetta M, Levitt MH (2010) Proc Natl Acad Sci USA 107:17135
159. Carravetta M, Johannessen OG, Levitt MH (2004) Phys Rev Lett 92:153003
160. Carravetta M, Levitt MH (2004) J Am Chem Soc 126:6228
161. Warren WS, Jenista E, Branca RT, Chen X (2009) Science 323:1711
162. Bowen S, Hilty C (2008) Angew Chem Int Ed Engl 47:5235
163. Harris T, Giraudeau P, Frydman L (2011) Chemistry 17:697
164. Bowen S, Sekar G, Hilty C (2011) NMR Biomed 24:1016–1022
165. Jensen PR, Meier S, Ardenkjaer-Larsen JH, Duus JO, Karlsson M, Lerche MH (2009) Chem Commun (Camb):5168
166. Lerche MH, Meier S, Jensen PR, Baumann H, Petersen BO, Karlsson M, Duus JO, Ardenkjaer-Larsen JH (2010) J Magn Reson 203:52
167. Joo CG, Hu KN, Bryant JA, Griffin RG (2006) J Am Chem Soc 128:9428
168. Ardenkjaer-Larsen JH, Laursen I, Leunbach I, Ehnholm G, Wistrand LG, Petersson JS, Golman K (1998) J Magn Reson 133:1
169. Thaning M (2000) US Patent 6,013,810
170. Wind RA, Ardenkjaer-Larsen JH (1999) J Magn Reson 141:347
171. Dane EL, Maly T, Debelouchina GT, Griffin RG, Swager TM (2009) Org Lett 11:1871
172. Gafurov M, Lyubenova S, Denysenkov V, Ouari O, Karoui H, Le Moigne F, Tordo P, Prisner T (2010) Appl Magn Reson 37:505
173. Gabellieri C, Mugnaini V, Paniagua JC, Roques N, Oliveros M, Feliz M, Veciana J, Pons M (2010) Angew Chem Int Ed Engl 49:3360
174. Paniagua JC, Mugnaini V, Gabellieri C, Feliz M, Roques N, Veciana J, Pons M (2010) Phys Chem Chem Phys 12:5824
175. Stephan M, Günther UL (PhosPhoenix SARL) Patent FR2010 04364
176. Dollmann BC, Kleschyov AL, Sen V, Golubev V, Schreiber L, Spiess H, Münnemann K, Hinderberger D (2010) Chemphyschem 11:3656
177. Dollmann BC, Junk MJN, Drechsler M, Spiess HW, Hinderberger D, Münnemann K (2010) Phys Chem Chem Phys 12:5879
178. Pavlovskaya GE, Cleveland ZI, Stupic KF, Basaraba RJ, Meersmann T (2005) Proceedings of the National Academy of Sciences of the United States of America 102:18275
179. Türke M-T, Bennati M (2011) Phys Chem Chem Phys 13:3630–3633
180. Barnes A, De Paëpe G, Van Der Wel P, Hu K, Joo C, Bajaj V, Mak-Jurkauskas M, Sirigiri J, Herzfeld J, Temkin R, Griffin R (2008) Appl Magn Reson 34:237

http://www.springer.com/978-3-642-37990-1

Modern NMR Methodology
Heise, H.; Matthews, S. (Eds.)
2013, VII, 204 p. 50 illus., 43 illus. in color., Hardcover
ISBN: 978-3-642-37990-1